

1 Evolution of the dynamics, area and ice production of the

2 Amundsen Sea Polynya, Antarctica, 2016-2021

3 Grant J. Macdonald^{1*}, Stephen F. Ackley¹, Alberto M. Mestas-Nuñez¹ and Adrià Blanco-Caba-
4 nillas²

5 1) NASA Center for Advanced Measurements in Extreme Environments (CAMEE), University of Texas at
6 San Antonio, San Antonio, TX 78249, USA

7 2) Department of Geography, University of Victoria, Victoria, BC V8W 2Y2, Canada

8 *Currently at (2)

9 *Correspondence to:* Grant J. Macdonald (grantmacdonald@uvic.ca)

10
11 **Abstract.** Polynyas are key sites of ice production during the winter and are important sites of biological activity
12 and carbon sequestration during the summer. The Amundsen Sea Polynya (ASP) is the fourth largest Antarctic po-
13 lynya, has recorded the highest primary productivity and lies in an embayment of key oceanographic significance.
14 However, knowledge of its dynamics, and of sub-annual variations in its area and ice production, is limited. In this
15 study we primarily utilize Sentinel-1 SAR imagery, sea ice concentration products and climate reanalysis data, along
16 with bathymetric data, to analyze the ASP over the period November 2016 - March 2021. Specifically, we analyze
17 (i) qualitative changes in the ASP's characteristics and dynamics, and quantitative changes in (ii) summer polynya
18 area, (iii) winter polynya area and ice production. From our analysis of SAR imagery we find that ice produced by
19 the ASP becomes stuck in the vicinity of the polynya and sometimes flows back into the polynya, contributing to its
20 closure and limiting further ice production. The polynya forms westward off a persistent chain of grounded icebergs
21 that are located at the site of a bathymetric high. Grounded icebergs also influence the outflow of ice and facilitate
22 the formation of a 'secondary polynya' at times. Additionally, unlike some polynyas, ice produced by the polynya
23 flows westward after formation, along the coast and into the neighboring sea sector. During the summer and early
24 winter, broader regional sea ice conditions can play an important role in the polynya. The polynya opens in all sum-
25 mers, but record-low sea ice conditions in 2016/17 cause it to become part of the open ocean. During the winter, an
26 average of 78% of ice production occurs in April-May and September-October, but large polynya events often asso-
27 ciated with high, south-easterly or easterly winds can cause ice production throughout the winter. While passive mi-
28 crowave data or daily sea ice concentration products remain key for analyzing variations in polynya area and ice
29 production, we find that the ability to directly observe and qualitatively analyze the polynya at a high temporal and
30 spatial resolution with Sentinel-1 imagery provides important insights about the behavior of the polynya that are not
31 possible with those datasets.

36 1. Introduction

37 Coastal polynyas, or ‘latent heat polynyas’ (and henceforth referred to simply as ‘polynyas’), are sites of
38 open water surrounded by sea ice and land, glacier ice, or fast ice (Armstrong, 1972; Tamura et al., 2008; Park et al.,
39 2018). These polynyas are distributed around the coast of Antarctica and are typically at fixed geographic locations
40 each year. They develop because the ice that forms at these sites is regularly driven away by winds or ocean cur-
41 rents, creating an opening in the sea ice (Bromwich and Kurtz, 1984; Bromwich et al., 1993; 1998; Morales
42 Maqueda et al. 2004; Sansiviero et al., 2017).

43 Between the Antarctic summer months of approximately November and March these open water sites tend
44 to remain persistently ice-free. Among other factors, the combination of ice-free conditions, summer sunlight, and
45 the availability of dissolved iron (e.g. Arrigo et al., 2008a; 2012; St-Laurent et al., 2017), enables large phytoplank-
46 ton blooms to develop in polynyas during this summer period. These phytoplankton blooms fix carbon from dis-
47 solved carbon dioxide, some of which then sinks below the surface layer (Sweeney et al., 2003). As a result, the evo-
48 lution of polynyas during the summer is considered a key factor in the primary productivity of the Southern Ocean,
49 and consequently, also their role in the sequestration of carbon dioxide (the ‘biological pump’) (Arrigo et al.,
50 2008b).

51 Between the Antarctic winter months of approximately April and October polynyas tend to be intermit-
52 tently active and are smaller in area than in the summer. When a polynya does open during the winter, excess ocean
53 heat is lost and new sea ice production takes place approximately immediately in the opened area. Winds (usually
54 katabatic winds) or ocean currents later push the newly-produced sea ice away and open the polynya again, causing
55 yet more ice to form. Repeated polynya ‘events’ produce new sea ice throughout the winter period and hence polyn-
56 yas have been termed ‘factories’ of sea ice production (Kimura and Wakatsuchi, 2004; Assmann et al., 2005). Over-
57 all, polynyas are estimated to contribute around 10% of all Antarctic sea ice cover (Tamura et al., 2008; Nihashi and
58 Oshima, 2015). Regionally, polynyas can play an even larger role in production. For example, the Ross Ice Shelf
59 polynya is estimated to produce several cubic kilometers of ice annually, and along with the McMurdo Sound Po-
60 lynya, may produce 20-50% of total sea ice in the region (Drucker et al., 2011). The polynya-produced ice then
61 forms part of the pack ice, contributing to its characteristics and potentially further thickening it due to deformation.
62 For example, ice formed by the Terra Nova Bay polynya in the western Ross Sea had a mean thickness 3-4 times
63 that of the central Ross Sea, with 80% of the ice contained in deformed ice and ridges (Rack et al., 2020). Conse-
64 quently, understanding of polynya evolution through the winter is important for understanding ice production and
65 sea ice characteristics in the Southern Ocean.

66 The Amundsen Sea Polynya (ASP), West Antarctica and the embayment in which it lies are of particular
67 interest for several reasons. The polynya is situated in the embayment into which the Thwaites and Pine Island Glac-
68 iers terminate and undergo ocean-driven melting, making the oceanography of the embayment of special interest
69 (IMBIE team, 2018; Rignot et al., 2019). The ASP is also known to be a key site of primary productivity in the sum-
70 mer, supporting rates of net primary production up to $2.5\text{gC m}^{-2}\text{ day}^{-1}$, the highest for any Antarctic polynya (Arrigo
71 and Van Dijken, 2003; Arrigo et al., 2012), although the level of associated carbon sequestration is unclear (Lee et

72 al., 2017; St-Laurent et al., 2019). Additionally, the ASP has been highlighted as an important site for ice produc-
73 tion. It has been identified as the fourth highest polynya in Antarctica in terms of area and ice production, only be-
74 hind the Ross Ice Shelf, Cape Darnley, and Mertz polynyas (Tamura et al., 2008; 2016; Nihashi and Ohshima, 2015,
75 Nihashi et al., 2017).

76 While there have been several recent studies of the ASP's evolution during the summer months (e.g. Arrigo
77 et al., 2012; Stammerjohn et al., 2015, St-Laurent et al., 2019), knowledge of the ASP and its role in ice production
78 during the winter is limited. Additionally, few studies during the summer have analyzed changes at the sub-monthly
79 scale, and none have observed the polynya directly during cloudy conditions. Aside from one study that analyzed the
80 ASP at the mean monthly scale (Tamura et al., 2016), studies that analyze ice production in the ASP during the win-
81 ter have been limited to estimates of total annual ice production and mean annual area as part of broader-scale cir-
82 cum-Antarctic studies (Tamura et al., 2008; Nihashi and Ohshima, 2015; Nihashi et al., 2017). Other studies of the
83 ASP during the winter have focused on other aspects of the polynya, such as iron and carbon fluxes (St-Laurent et
84 al., 2019). There are a lack of studies of the polynya that characterize changes in the polynya's evolution and area
85 through individual seasons. This is partly due to the difficulty of analyzing polynyas in detail during the polar night.
86 However, the launch of the Sentinel-1 constellation of Synthetic Aperture Radar (SAR) - in full operation by May
87 2016 - enables us to directly observe the polynya during the polar night at a high spatial resolution. Additionally,
88 during the summer light, SAR allows us to make observations regardless of cloud cover.

89 The overall goal of the work presented here is to improve knowledge of the behavior and evolution of the
90 ASP, and thus to aid understanding of recent complex and poorly understood trends in Southern Ocean sea ice con-
91 ditions. This in turn, will aid projections of future changes in Southern Ocean sea ice condition due to climate
92 change, with important consequences for a range of processes such as Antarctic Ice Sheet stability (Banwell et al.,
93 2017; Webber et al., 2017; Greene et al., 2018; Massom et al., 2018; Arthur et al., 2021) and ecosystem productivity
94 (Grossman and Dieckmann, 1994; Ito et al., 2017). In particular we aim to provide the first qualitative description
95 of the polynya's behavior based on direct observation. The three specific objectives of this paper are to, over the pe-
96 riod November 2016 - March 2021, analyze seasonal and inter-annual (i) qualitative changes in the ASP's character-
97 istics and dynamics, and quantitative changes in (ii) summer polynya area and (iii) winter polynya area and ice pro-
98 duction. The main datasets used are Sentinel-1 SAR images, sea ice concentration products, and climate reanalysis
99 data in the region of the ASP. Additionally, we analyze bathymetric data, and changes in the broader regional sea
100 ice.

101 102 **2. Study Site**

103 The ASP is located at around $\sim 72\text{-}73^\circ\text{S}$ and $110\text{-}120^\circ\text{W}$ in the Amundsen Sea embayment of the Southern
104 Ocean in West Antarctica (Fig. 1). It is situated in a sector that exhibited an anomalous 40-year decreasing trend in
105 sea ice extent until a 2007 minimum, since which there has been an increasing trend (Parkinson, 2019). The embay-
106 ment also hosts an abundance of icebergs (Mazur et al., 2017; 2019; Bett et al., 2020). To the east, the polynya is
107 bound by the Thwaites Iceberg Tongue (Iceberg B22A; Budge and Long, 2018) and a chain of icebergs grounded
108 over Bear Ridge. To the south, when at its maximum extent, the polynya abuts the Dotson Ice Shelf and part of the

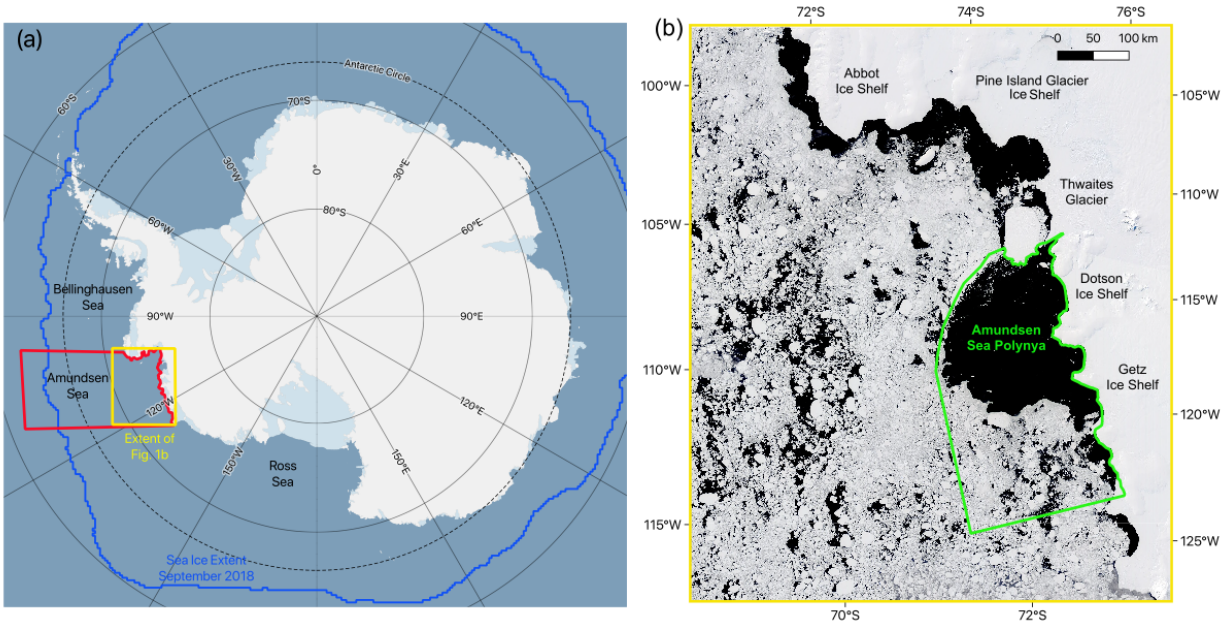
109 Getz Ice Shelf. Immediately east of the eastern boundary of the polynya is an area of ocean that is adjacent to
110 Thwaites Glacier and Pine Island Glacier. The neighboring 'Pine Island Polynya' forms along the coastal stretch
111 around this area and to the north. Westward coastal currents prevail in the area (Kim et al., 2016; St-Laurent et al.,
112 2019), that, along with easterly winds, carry icebergs (Koo et al., 2021) and sea ice into the adjacent sector or the
113 Amundsen Sea and eventually to the Ross Sea (Assmann et al., 2005).

114 The ASP opened every summer during the period 1979-2014 studied by Stammerjohn et al. (2015) and re-
115 tained some open polynya area through the winter period. Arrigo et al. (2012) found no significant secular trend in
116 mean summer open water area between 1997 and 2010, but Stammerjohn et al. (2015) did find the ASP's area in
117 December-February to increase overall over the period 1979-2014. They also noted that the site of the polynya
118 opening shifted to its current typical site adjacent to the Thwaites Glacier Tongue in 1993, having previously been
119 further to the west.

120 Synoptic-scale winds have been found to primarily determine the ASP's area and the timing of opening and
121 closure. Over the period 1997-2010, ASP area was greatest in the summers of 2002-03 and 2009-10, the years with
122 the largest monthly anomalies in easterly and southerly surface winds in the region, and smallest in 2003-04 when
123 there were anomalously high northerly and westerly winds (Arrigo et al., 2012). Polynya summer opening in No-
124 vember was associated with prevailing easterly or southeasterly winds, while closure in March was associated with
125 persistent southeasterly winds at a time when winds promote ice growth in open areas. The polynya was also found
126 to open for summer 16 ± 7 days earlier at the end of the period 1979/80-2013/14 than the beginning (Stammerjohn
127 et al., 2015).

128 During the winter, the ASP active area was estimated to have a daily mean of 7700 ± 3600 km² for the pe-
129 riod March-October, 2003-11, as estimated by mapping thin-ice thickness from Advanced Microwave Scanning Ra-
130 diometer for EOS [Earth Observing System] (AMSR-E) data (Nihashi and Ohshima, 2015). Annual ice production
131 volume has been estimated as 92 ± 16 km³ for the period 1992-2001 (Tamura et al., 2008) and 123 ± 24 km³ for the
132 period 1992-2013 (Tamura et al., 2016) by mapping thin-ice thickness using Special Sensor Microwave/Imager
133 (SSM/I) data and calculating heat flux using SSM/I and surface atmospheric data. Nihashi et al., 2017 estimated an-
134 nual volume of ice production, as 90 ± 13 km³ for the period 2003-10, and 90 ± 17 km³ for the period 2013-15 , by
135 mapping thin-ice thickness and estimating heat fluxes using AMRS-E and AMSR2 data, respectively.

136



137
 138 **Fig. 1.** (a) The location of the Amundsen Sea and our study sites within the context of Antarctica and the Southern
 139 Ocean. The background image is from Quantarctica (Matsuoka et al., 2021); (b) The location of the ASP within the
 140 Amundsen Sea embayment. The green boundary indicates the area defined as the ‘ASP study area’ for the purpose
 141 of calculating winter polynya area and ice production. The background image is a true-color MODIS image from 12
 142 December 2020.
 143

144 **3. Data & Methods**

145 **3.1 Qualitative analysis of the ASP’s evolution**

146 In order to qualitatively characterize the seasonal and interannual evolution of the ASP we use Sentinel-1
 147 SAR imagery. Qualitative visual analysis allows us to identify dynamics that are not easy or possible to identify
 148 and/or describe with quantitative data. Sentinel-1 is a constellation of two satellites, A and B, that were launched by
 149 the European Space Agency (ESA) in 2014 and 2016, respectively. The satellite collects radar backscatter imagery
 150 in the C-band which allows observations of sea ice and the ocean during cloudy conditions and the polar night.

151 For our analysis we produced a time-lapse animation in Google Earth Engine using all Sentinel-1 extra-
 152 wide swath (EW) mode, Ground Range Detected (GRD) images over the study site, described in section 2, and its
 153 surroundings for the period November 2016 to March 2021. This period was chosen because it includes all the com-
 154 plete summer (November-March) and winter (April-October) periods during which both satellites A and B of the
 155 Sentinel-1 SAR constellation have been active. The EW mode was primarily designed for sea ice and polar zones
 156 and collects images over a wider area than other modes. EW images are available in 20m x 40m spatial resolution
 157 and all images were resampled to 40 m grid spacing. Of four available band combinations (VV, HH, VV+VH, and
 158 HH+HV), we use the HH band because most of the images contain this band. Google Earth Engine applies a series
 159 of pre-processing steps to Sentinel-1 images (<https://developers.google.com/earth-engine/guides/sentinel1>): 1) appli-
 160 cation of orbit file, 2) GRD border noise removal, 3) thermal noise removal, 4) radiometric calibration and 5) or-
 161 thorectification. Images are also converted to decibels (dB). Using these images, we created a time-lapse animation
 162 using Google Earth Engine. This time-lapse included at least partial coverage of the study area for 56 days in 2016,

163 359 days in 2017, 341 days in 2018, 317 days in 2019, 329 days in 2020 and 85 days in 2021. In order to analyze
164 particular images in detail, the images were also downloaded from the Alaska Satellite Facility (asf.alaska.edu) and
165 processed in ESA's 'SNAP' toolbox. SNAP was used to crop the images, apply radiometric correction (gamma-
166 nought), apply a Lee (7 x7) speckle filter, and perform ellipsoid correction and map projection, projecting to an Ant-
167 arctic polar stereographic projection. These images were also converted to decibels. The images were then loaded
168 into QGIS (QGIS.org, 2021) for analysis.

169 Qualitative analysis was carried out by visually analyzing the time-lapse videos and images of interest, not-
170 ing changes in the state of the polynya and ice in the region. Visual analysis is possible by analyzing changes in the
171 backscatter signal's texture, pattern, and tone and because of the distinct backscatter characteristics of open water,
172 older icepack and different types of thin sea ice. The motion of the ice between images also helped in the identifica-
173 tion of polynya events. Numerous previous studies have noted the ability to observe polynya activity and visually
174 identify polynya opening and the drift of ice with SAR imagery and Sentinel-1 in particular (e.g. Hollands and
175 Dierking, 2016; Dai et al., 2020; Moore et al., 2021). Visual qualitative analysis of SAR imagery also forms an im-
176 portant part of, for example, the Environment Canada's production of sea ice charts (Environment Canada, 2005).
177 Typically, open ocean water has a low backscatter and appears dark, while thicker, older icepack has a relatively
178 high backscatter and appears bright and more granular (we refer to all ice not produced by the ASP as 'pack ice')
179 (Fig. 2a-b). Recently-formed polynya-produced ice has an intermediate backscatter (Fig. 2a). Frazil ice, that may
180 form when a polynya opens up and the open ocean begins to freeze, typically forms in distinct bands of varying
181 brightness (Fig. 2c-d) although it may also form in a 'swirl' or other forms. Open ocean may also appear bright dur-
182 ing high winds, but it is typically clear from the pattern, tone, and texture, and the context of the image whether it is
183 an area of ice-free open ocean, or an area of pack ice or active polynya. Incidence angle also influences backscatter
184 and should be considered particularly in a quantitative study of backscatter, but it is not generally considered a sig-
185 nificant impediment in the ability to qualitatively analyses the images for this study's purpose, with visual analysis
186 dependent on a number of factors. Note that what we refer to as 'active' polynya area during the winter will typi-
187 cally be filled with thin, newly-forming frazil ice.

188 Given the role grounded icebergs play in bounding the ASP, we also downloaded the 'BedMachine Antarc-
189 tica V2' sea floor topography dataset for our study area to examine alongside our qualitative analysis. This dataset
190 was downloaded from the NSIDC (<https://nsidc.org/data/nsidc-0756>) and has a grid spacing of 500 x 500 m
191 (Morlighem et al., 2020).

192 We also use our analysis of the imagery to assess the approximate day of summer polynya 'opening' and
193 'closing'. We deem the polynya to be open for the summer when the open polynya area is primarily free of active
194 ice production, and the day of summer closing to be when the whole open polynya is subject to ice production.

195 196 **3.2 Daily polynya area**

197 In order to analyze seasonal and interannual changes in polynya area in summer and winter, daily sea ice
198 concentration (SIC) for the study region was downloaded from the University of Bremen's sea ice data center
199 (seaice.uni-bremen.de). The data was separated into five summer periods from November to March (2016/17,

200 2017/18, 2018/19, 2019/20 2020/21) and four winter periods from April to October (2017, 2018, 2019, 2020). This
201 time period was focused on because it coincides with the period for which there is Sentinel-1 A and B data. During
202 the winter we use the term ‘active polynya’ for areas that we include in the polynya, where an opening has been cre-
203 ated and new ice production is taking place. During the winter we expect thin, frazil ice to immediately begin form-
204 ing when an opening is created (e.g. Nakata et al., 2019; 2021), and thus we prefer the term ‘active’ to ‘open’ po-
205 lynya. We begin our winter period in April rather than March because analysis of the Sentinel-1 imagery suggests
206 ice production is not typically active across the open polynya at the beginning of March. The sea ice concentration
207 product was processed by the University of Bremen using the ARTIST Sea Ice (ASIC) algorithm (Spren et al,
208 2008) applied to AMSR-2 data. AMSR-2 was launched onboard the Japan Aerospace Exploration Agency’s (JAXA)
209 Global Change Observation Mission – Water (GCOM-W) satellite in July 2012.

210 We used version 5.4 of the Antarctic-wide, daily sea ice concentration product with no land mask, pro-
211 cessed to 3.125 km grid spacing. This is of a higher-resolution than data previously used to analyze polynya area in
212 the region. For example, Arrigo et al., (2012) used SSM/I data with 6.25 km grid spacing for their study of summer
213 polynya area. Nihashi et al. (2017) used AMSR-E data with 6.25 km grid spacing for their estimates of ice produc-
214 tion. Tamura et al. (2008; 2016) also used SSM/I data, with 12.5 km grid spacing, for estimates of ice production.
215 Stammerjohn et al. (2015) used Bootstrap SIC data with 25 km grid spacing for their analysis of summer polynya
216 area. However, with our higher-resolution data (3.125 km) there remain limitations in using data with such a scale to
217 measure something that can vary on a meterscale. It has been estimated that the ice concentration error in our
218 AMSR-2 dataset is 25% at 0% SIC, decreasing to <10% error for SIC over 65% and 5.7% error at 100% SIC
219 (Spren et al., 2008). It is also noted that the SIC data is known to underestimate SIC where there is thin ice, but as
220 we define an active polynya as including thin ice, this is not likely to lead to substantial misclassification of active
221 polynya areas. The data may also incorrectly classify stable fast ice as being an area of low SIC, but we exclude
222 these areas from the study area. Data was available for all days in our study period apart from one day in 2019 (1
223 September).

224 After each day’s data was downloaded as a geotiff, it was cropped to the 70 660 km² ASP study area de-
225 fined in Fig. 1b using a shapefile drawn in QGIS with a Sentinel-1 image as reference. Polynya area was then calcu-
226 lated by defining any pixel in the study area with a SIC < 70% as being part of the open/active polynya. The 70%
227 threshold has been commonly used in other studies of polynyas in the summer (e.g. Parmiggiani, 2006; Morelli &
228 Parmiggiani, 2013; Preußner et al., 2015), and the approach has also been used before to calculate winter polynya
229 area (Cheng et al., 2017; 2019). A limitation is that smaller areas of open water that are represented in a pixel domi-
230 nated by ice-covered area (i.e. > 70%) will not be included in our polynya area value, while ice-covered areas in pix-
231 els with SIC < 70% will be included. However, by comparing our SIC data with the SAR imagery we found apply-
232 ing a 70% threshold to the SIC data an effective way of capturing winter, as well as summer, polynya area in our
233 study area. For example, Fig. 2 b-d shows SAR imagery for a section of the polynya on 21-23 September 2020 and
234 e-g shows the active polynya as identified using a 70% threshold with the SIC data for the same days. To further
235 compare the identification of active winter polynya as identified using SIC data with the SAR imagery, we manually
236 identified active polynya in the SAR imagery for the nine days in 2020 when SAR imagery covers the whole ASP

237 study area (green box in Fig. 1b). The results of the comparison can be seen in Fig S1 and generally show good
238 agreement. Note that even if the method was perfect there would be a discrepancy because the measurements are
239 taken at different times of day and significant changes in active area can occur in hours due to movement of ice,
240 freezing, or a mixture of processes. There is also an element of human error in the manual measurement. Of the nine
241 cases, the area was identified as higher using SIC data in five cases and using SAR data in four cases, suggesting
242 that neither approach leads to a systematic over-estimation. Observing Video S2 in comparison to available images
243 in Video S1 also shows the SIC typically effectively captures the presence, and variations in area of, the active po-
244 lynya.

245 While Sentinel-1 imagery has been used to obtain polynya area during the polar night at a higher spatial
246 resolution (40m, Dai et al., 2020), the Bremen SIC product has three key advantages over using Sentinel-1 SAR im-
247 agery. First, the SIC product is available daily, in contrast to Sentinel-1 which has many, and sometimes prolonged,
248 data gaps over the primary area of interest, particularly during June/July. Given that polynya area can change sub-
249 stantially on a daily or hourly timescale, regular gaps of successive days significantly limits the ability to quantita-
250 tively characterize variations throughout the year. Second, several Sentinel-1 images are required to capture the
251 whole ASP study area on a particular day, meaning that even on many days where there are images that are useful
252 for qualitative analysis, the whole polynya cannot be measured. For example, in 2020 there is full coverage of the
253 whole ASP study area for only 22 days with none between 26 April and 12 August, and 9 days in winter (although
254 there are many other days when the whole of the actual open/active polynya itself is visible as it does not extend
255 throughout the whole study area). Third, even if sufficient images were available, current methods for calculating
256 polynya area in Sentinel-1 imagery (e.g. Dai et al., 2020) requires manual delimitation, which is labor intensive and
257 would be highly time consuming to do for multiple years at a daily temporal resolution. Automated detection of ac-
258 tive polynya area in winter using SAR is not yet possible to our knowledge.

259

260 **3.3 Daily winter ice production**

261 In order to calculate daily ice production in the ASP during the winter periods we followed the approach of
262 Cheng et al. (2017) and utilized their heat flux and ice production model. As input to the model we used atmospheric
263 re-analysis data from the European Centre for Medium-Range Weather Forecasts Reanalysis v5 (ERA5) and the
264 same sea ice concentration data from the University of Bremen described in section 3.2.

265 Hourly ERA5 data, with a spatial resolution of 31 km, was downloaded from Copernicus (cds.climate.co-
266 pernicus.eu; Herbach et al., 2018) for the following meteorological variables: air temperature at a height of 2 m,
267 wind speed at a height of 10 m, surface air pressure, dewpoint temperature at a height of 2 m, downward solar radia-
268 tion and downward thermal radiation. Air temperature, wind speed, surface air pressure and dewpoint temperature
269 were then processed to daily mean values, while solar and thermal radiation were processed to daily cumulative val-
270 ues. These calculations were done for the same ASP study site as for polynya area (Fig. 1b).

271

272 **3.3.1 Heat Flux Calculation**

273 Following Cheng et al. (2017) the daily net heat flux, Q (in Wm^{-2}), of an active-polynya pixel was esti-
274 mated by:

$$275$$
$$276 \quad Q = (1 - \alpha)R_i + L_i - L_o + F_s + F_e \quad (1)$$

277
278 where R_i (in Wm^{-2}) is the cumulative downward solar radiation; L_i (in Wm^{-2}) is the cumulative downward thermal
279 radiation; L_o (in Wm^{-2}) is the upward thermal radiation; F_s (in Wm^{-2}) and F_e (in Wm^{-2}) are the sensible heat flux
280 and latent heat flux, respectively; and α is the albedo of open water. α was taken to be 0.06 following Cheng et al.
281 (2017; 2019), R_i and L_i were taken from the processed daily ERA5 values and L_o , F_s and F_e were calculated as de-
282 scribed below.

283 The upward thermal radiation was calculated by the Stefan-Boltzmann law:

$$284$$
$$285 \quad L_o = \varepsilon\sigma T_s^4 \quad (2)$$

286
287 where ε is the longwave emissivity of open water (0.99), and σ is the Stefan-Boltzmann constant (5.67×10^{-8}
288 $\text{W}^{-2}\text{K}^{-4}$). The temperature of the water surface (T_s , in K), was assumed to be at the freezing point of seawater (T_0 in
289 K), which was calculated following Doherty and Kester (1974) and Cheng et al. (2017; 2019) as:

$$290$$
$$291 \quad T_s \sim T_0 = 273.15 - 0.0137 - 0.05199S_w - 0.00007225S_w^2 \quad (3)$$

292
293 where S_w (in ‰) is the salinity of sea water. The salinity of the Amundsen Sea was estimated as 34‰ based on Bett
294 et al. (2020).

295 The sensible heat flux, (F_s), and latent heat flux, (F_e) was calculated by:

$$296$$
$$297 \quad F_s = \rho_a c_p C_s U (T_a - T_0) \quad (4)$$

298
299 and

$$300$$
$$301 \quad F_e = 0.622\rho_a L_v C_e U (r e_a - e_s) / P_0 \quad (5)$$

302
303 where ρ_a is the density of air at standard atmospheric pressure and 0°C, taken as, 1.3 kg m^{-3} , c_p is the specific heat of
304 air at constant pressure, taken as $1004 \text{ J kg}^{-1} \text{ K}^{-1}$, U (in ms^{-1}) is the wind speed at 10 m, taken from the processed
305 ERA5 data and T_a (in K) is the air temperature at 2 m, taken from the processed ERA5 data. C_s and C_e are bulk
306 transfer coefficients for sensible heat and latent heat, respectively and both taken as 0.00144. P_0 (in Pa) is the sur-
307 face air pressure and taken from the processed ERA5 data. L_v (in J kg^{-1}) is the latent heat of water vaporization, r is
308 the relative humidity. E_a (in Pa) is the saturation water vapor pressure at the air temperature, $r e_a$ is the actual water

309 vapor pressure of the air and e_s (in Pa) is the saturated water vapor pressure at the surface temperature and are all
310 calculated below:

311

$$312 \quad L_v = [2.501 - 0.00237(T_s - 273.15)] \times 10^6 \quad (6),$$

313

$$314 \quad e_s = 611.21 \times 10^{9.8094(T_s - 273.15)/(T_s + 0.71)} \quad (7),$$

315

316 and

317

$$318 \quad re_a = 611.21 \times 10^{9.8094(T_d - 273.15)/(T_d + 0.71)} \quad (8)$$

319

320 where T_d is the dewpoint temperature taken from the processed ERA5 data.

321

322 3.3.2 Ice production calculation

323 The calculated daily heat flux was then cropped, re-aligned, resampled to a 3.125 km² grid and reprojected

324 to Antarctic Polar Stereographic using GDAL (Geospatial Data Abstraction Library) and QGIS to match the corre-

325 sponding sea ice concentration data. Next, where SIC was < 0.7 (i.e. pixels considered as part of active polynya)

326 daily ice production volume, V , was estimated in km³ following Cheng et al. (2017) by the following equation (9).

327 Although ice production will also take place in non-polynya areas where there is ice cover, here we are only con-
328 cerned with ice production taking place in the active polynya.

329

$$330 \quad V = 3.125^2(1 - SIC)Q/\rho_i L_f \quad (9)$$

331

332 where, as above, SIC is sea ice concentration (as a fraction) and Q is daily net heat flux in W m⁻², ρ_i is sea ice den-

333 sity and taken as 920 kg m⁻³ and L_f is the latent heat of sea ice fusion in J kg⁻¹. L_f is calculated following Moham-

334 med and Nirmal (2015) and Cheng et al. (2017) by:

335

$$336 \quad L_f = 333400 - 2113(T_0 - 273.15) - 114S_i + 18040S_i/(T_0 - 273.15) + 3.35S_i(T_0 - 273.15) - 3.76(T_0 - 273.15)^2 \quad (10)$$

337

338 where S_i is the salinity of sea ice, taken as 6‰ following Cheng et al. (2017).

339 Caution should be used when interpreting the absolute numbers produced by the ice production model, par-

340 ticularly because the input data is reanalysis data not necessarily always representative of reality. This is so because

341 the re-analysis itself is a simulation sensitive to uncertain parameter settings, although it is partly corrected by as-

342 sssimilation of observational data (Cheng et al., 2017; 2019). Also note ERA5 includes a prescribed ‘sea ice area frac-

343 tion’ parameter that influences the interaction between the atmosphere and ocean in the reanalysis. Nevertheless, we

344 opted for this method due to the difficulty of directly measuring and tracking thin ice thickness in the polynya (e.g.

345 Tian et al., 2020) to estimate ice production, and the potential to compare our daily ice production results to results
346 obtained by the same model for the Ross Ice Shelf Polynya (Cheng et al., 2017; 2019).

347

348 **3.4 Broader spatial changes in SIC**

349 In order to assess changes in the ASP in the context of changes in SIC at a broader spatial scale, SIC was
350 analyzed for the larger area defined in Fig. 1a. The same SIC dataset described in section 2.2 to obtain polynya area
351 was cropped to the broader region. The daily data was plotted spatially for all available days 1 November 2016 – 31
352 March 2021, as shown in Video S2. Monthly mean SIC was also calculated for the whole period and plotted spa-
353 tially. Additionally, the total SIC for each day was calculated by calculating the sum of all percentage SIC values in
354 the study region. These total SIC values should only be considered useful for analyzing relative changes in SIC in
355 our study period.

356

357 **3.5 Wind analysis**

358 In order to analyze the polynya’s behavior, we also considered wind conditions. Although a thorough anal-
359 ysis of wind-vector/ice property correlations is beyond the scope of the present paper, which is primarily focused on
360 estimating and describing the variability of the polynya’s dynamics, area and ice production, we do consider wind
361 conditions to help inform our analysis of the polynya. Mean daily and annual wind speed and vector winds were cal-
362 culated from hourly ERA5 reanalysis wind products. Hourly zonal (u) and meridional (v) components of vector
363 winds at a height of 10 m were obtained from ERA5 for a region adjacent to the Dotson Ice Shelf and iceberg chain
364 where the polynya typically forms, identified in Fig. S2. Hourly wind speed (V) in ms^{-1} and wind direction (θ) in
365 degrees were calculated as

366

$$367 \quad V = (u^2 + v^2)^{1/2} \quad (11)$$

368 and

$$369 \quad \theta = \tan^{-1} (v/u) \quad (12),$$

370

371 respectively. Daily averaged vector wind fields superimposed on maps of daily averaged wind speed were plotted
372 for the whole study area for the period 1 November 2016 to 31 December 2020 and are included as supplementary
373 video Video S3. A wind rose (Fig. 8) showing the wind speed and direction at times when the active polynya both
374 did not and did increase in area during winter (2017-2020) was also produced for the smaller area (shown by Fig.
375 S2) where the polynya forms from. A map of annual mean vector wind field superimposed on a map of annual mean
376 wind speed was plotted in Fig. 9.

377

378 Unfortunately, there is a lack of local observations of wind data in and around the study area with the clos-
379 est station in the United States Antarctic Program’s database, on Bear Peninsula, lacking wind data for most of our
380 study period. As a result, some caution should be employed when considering the results obtained from ERA5
381 winds. However, Bracegirdle (2013) and Stammerjohn et al. (2015) note that data from ERA5’s predecessor ERA-I
in the neighboring Bellingshausen Sea performed better than other reanalysis products.

382

383 **4. Results**

384 In this section, we first summarize our qualitative analysis of the polynya dynamics using Sentinel-1 SAR
385 imagery (Video S1) of the ASP between November 2016 and March 2021 (Section 4.1). Second, we analyze quanti-
386 tative changes in summer (November – March) polynya area for the summers of 2016/17 to 2020/21 (Section 4.2).
387 Third, we analyze quantitative changes in winter (April – October) polynya area and ice production for the winters
388 of 2017 to 2020 (Section 4.3). Fourth, we analyze spatial and temporal wind variations and how they relate to po-
389 lynya area (Section 4.4), and finally, we analyze broader regional patterns in sea ice concentration for the period No-
390 vember 2016 – March 2021 (Section 4.5).

391

392 **4.1 Qualitative analysis of ASP using Sentinel-1 SAR imagery**

393 Typically, in November or early December the polynya transitions from a winter into summer ‘mode’ as it
394 expands to the west and ice production ceases to take place in the open area i.e. the open polynya area is occupied
395 by open ocean rather than frazil or grease ice (Table 1, Video S1, e.g. Fig 1b). While the polynya’s eastern and
396 southern boundaries remain fixed at the Iceberg Chain and coast, respectively, at times during the summer the po-
397 lynya becomes unbound to the west and/or north, and consequently congruent with the open ocean. In the summers
398 of 2018/19 and 2019/20 it remains bound, but in 2016/17 and 2017/18 substantial openings develop in the pack ice
399 boundary. In the summer of 2016/17, particularly from December, the pack ice in the region is notably sparse in
400 comparison to the other years.

401 In February the pack ice around the polynya becomes more extensive and compact, predominantly due to
402 inflow from the Bellingshausen Sea in the north east. As the new pack ice flows into the area it reforms a west-
403 ern/northern boundary to the polynya in the years where a gap had opened, and in all years pushes the existing pack
404 to the east and south-east, reducing the polynya’s size. In the exceptionally low-pack ice summer of 2016/17, the
405 newly formed boundary of pack ice is remarkably narrow. In March in all years, new ice production can be seen
406 forming in parts of the polynya and is taking place across all of the polynya by the end of March or early April,
407 marking the polynya’s transition into winter ‘mode’ (Table 1).

408 Throughout the winter, polynya ‘events’ occur, with existing ice moving away, predominantly to the west
409 off the Iceberg Chain and Thwaites Iceberg Tongue, and new ice forming in the opening (e.g. Figs. 2b-d). On occa-
410 sion the polynya instead forms to the north off the Dotson Ice Shelf. Between April and August, the main polynya
411 appears to primarily have its maximum extent confined to the area adjacent to the Dotson Ice Shelf. Observation of
412 available imagery of polynya events, along with observation of newly-formed polynya ice outflowing from the area,
413 suggests that there is relatively low ice production in these deep winter months. Early and late in the winter, polynya
414 events are sometimes larger, extending further to the west, and there appears to be more associated ice production.

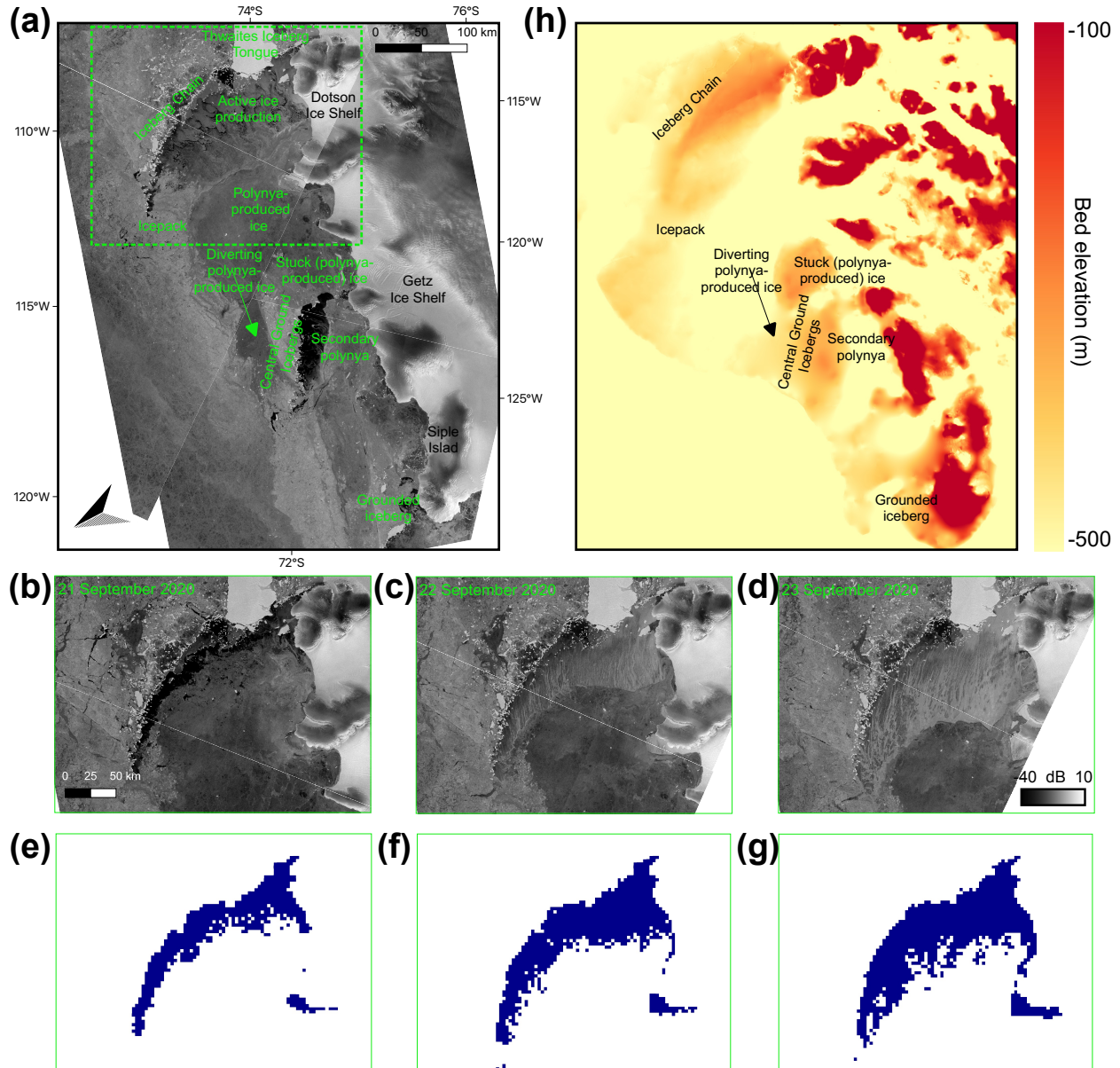
415 After early winter (March/April), as the area becomes more densely covered by inflowing pack ice and
416 newly-formed polynya ice, obstructions occur that appear to limit the evacuation of polynya-produced ice from the
417 vicinity and limit growth of the polynya. Obstructions particularly take place around and adjacent to a group of per-

418 sistently stuck icebergs around the center of the study area that we call the Central Grounded Icebergs around a sea-
419 floor high (Fig. 2a, h). New ice also sometimes becomes stuck (fast) directly adjacent to the south-west of this site
420 (Fig. 2a, h) on another sea-floor high. This intermittently-fast ice blocks outflow from the polynya to the west along
421 the coast, and at times forces new polynya-produced ice to divert around the north of Central Grounded Icebergs
422 (Fig. 2a). An area of grounded icebergs and intermittently-fast ice by Siple Island also sometimes obstructs ice and
423 causes diversions further to the north. All ice produced by the polynya flows to the west overall, eventually rounding
424 the corner of Siple Island.

425 We also observe that, while the overall flow of ice from the ASP is to the west, ice flowing from the po-
426 lynya through the winter ‘heaves’ and regularly temporarily reverses direction, ‘backfilling’ eastward into and to-
427 wards the polynya (e.g. Fig 3). This means the polynya sometimes closes through backfilling, and not only through
428 formation and growth of new ice. Back-filling also occur when the polynya does not appear open, meaning that raft-
429 ing and deformation presumably occurs as ice moves back into the polynya zone.

430 A series of smaller polynyas, other than the main polynya that forms off the Iceberg Chain and Dotson Ice
431 Shelf, also form within the study area at times. Mostly notably a ‘secondary polynya’ forms at times off the Central
432 Grounded Icebergs (Fig. 2a). With inflow of ice from the ASP to this area at times obstructed, as ice moves away
433 from the Central Grounded Icebergs to the west, an opening is created and active ice production is visible. Small
434 polynyas also form at times to the west off the outcrops along the coast.

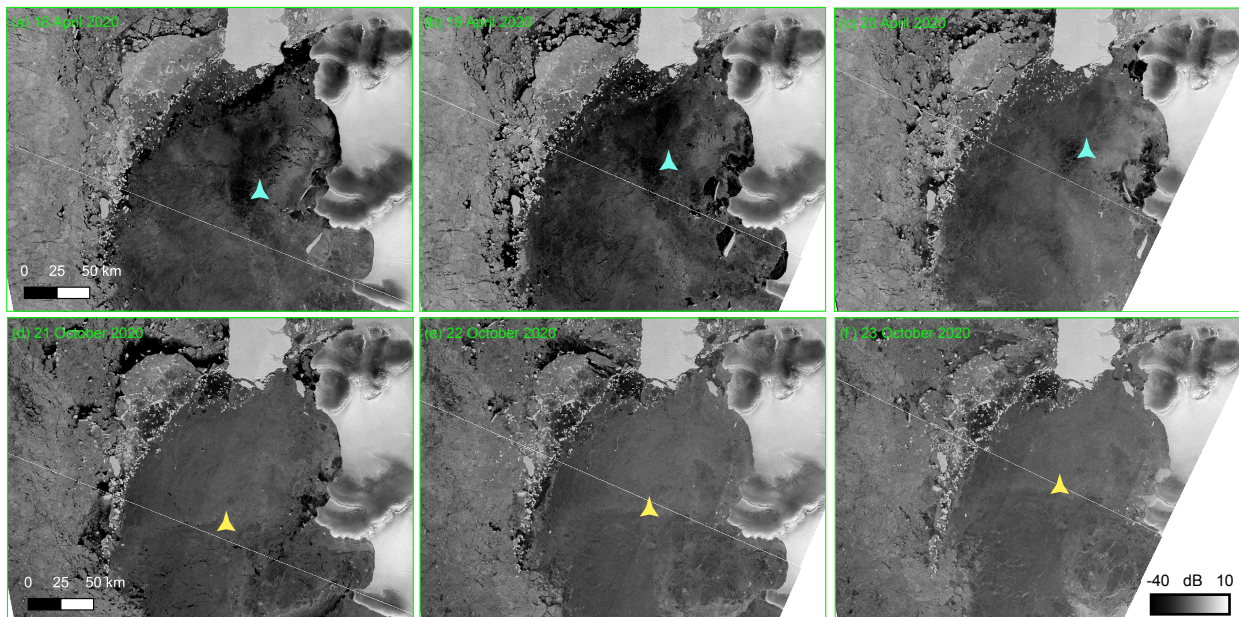
435



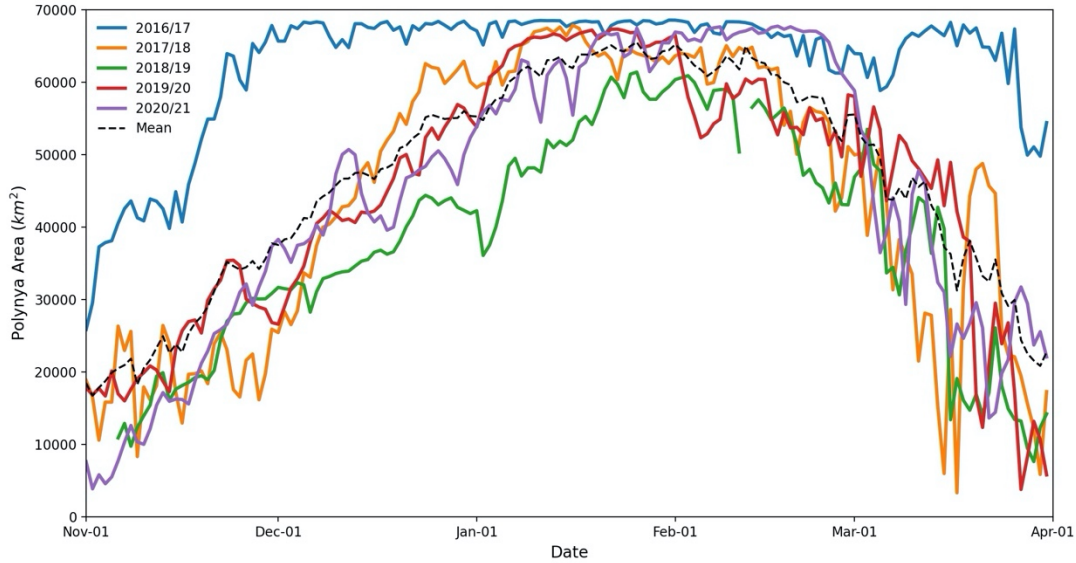
436
 437 **Fig. 2.** (a) An example image of the ASP during the winter in a Sentinel-1 SAR image from 5 September 2019. (b-
 438 d) An example of an active polynya event taking place 21-23 September 2020 in Sentinel-1 SAR imagery. Darker
 439 ice produced by the ASP can be seen diverting around the Central Grounded Icebergs (and some fast pack ice) after
 440 ice became stuck and obstructed outflow along the coast. The area corresponds to the dashed-green box in (a). (e-g)
 441 Active polynya area (blue) for the same dates and areas as b-d as measured by using a 70% threshold with SIC data
 442 (h) The elevation of the bed referenced to mean sea level for the same area as (a). The bathymetry data is from the
 443 MEaSUREs BedMachine version 2 dataset (Morlighem et al., 2019).
 444
 445

Year	Polynya opens	Polynya closes
2016/17	8 November 2016*	4 April 2017
2017/18	3 December 2017	9 March 2018
2018/19	13 November 2018	14 March 2019
2019/20	20 November 2019	21 March 2020
2020/21	16 November 2020	8 March 2021

446
447 **Table 1.** Summer polynya opening and closing dates for each summer 2016/17-2020/21 as determined by visual
448 analysis of Sentinel-1 SAR imagery. We determine the polynya to be open for summer when the majority of the
449 open polynya is not exhibiting ice production and closed when the majority of the polynya is exhibiting ice produc-
450 tion. * in 2016/17 a lack of imagery in early November means it is difficult to determine when the polynya opened,
451 but it is open by 8 November.
452



453
454 **Fig. 3** Examples of ‘back-filling’, ice earlier produced by the ASP flowing back towards the area adjacent to the Ice-
455 berg Chain where it formed. Each box corresponds to the same area shown by the dashed-green box in Fig. 2a, (a-c)
456 show the area on 18-20 April 2020, (d-f) show 21-23 October 2020. The colored shapes in each image are in ap-
457 proximately the same relative position within the ice in each set of images and are to help the reader spot the move-
458 ment of the ice through the movement of adjacent features. Other examples of back-filling are visible in Video S1.
459
460



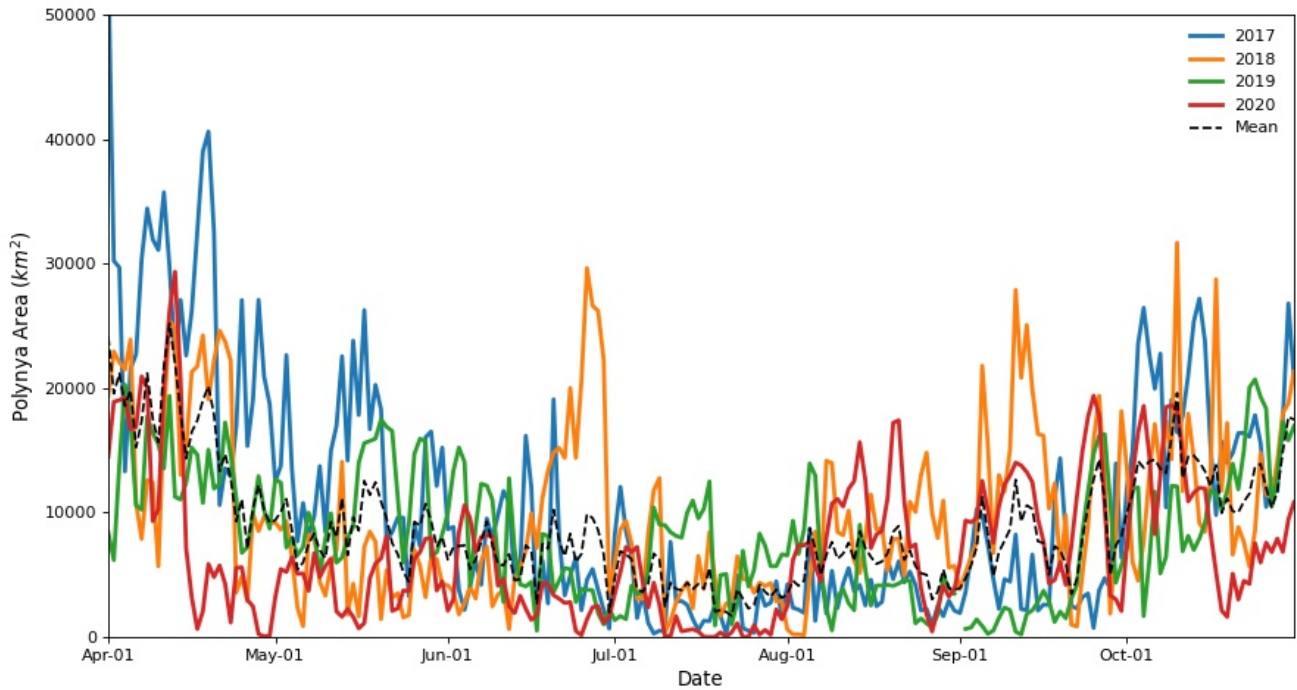
461
 462 **Fig. 4.** Daily summer (November-March) polynya area for each summer 2016/17-2020/21 (solid), and the 5-year
 463 mean of the daily areas for the whole summer period (dashed).
 464

465
 466 **4.2 Summer Polynya Area**

467 In all years there is an overall increase in polynya area through November (Fig 4). On 1 November, the po-
 468 lynya has an area between 7 617 km² (2020) and 25 859 km² (2016). In the years 2017/18, 2018/19, 2019/20 and
 469 2020/21 the polynya area follows a similar pattern, but in 2016/17 it follows a distinct course. By 1 December in
 470 2016 the polynya is open in approximately the whole ASP study area, with an area of 65 674 km², an increase of
 471 154% from 1 November. In 2016/17 the polynya remains open across approximately the whole study area through-
 472 out December, January, and most of February and March, only beginning to significantly decline in late March (Fig
 473 4) and into April (Fig 5). The polynya in 2016/17 maintains a higher area than in all other years throughout the
 474 whole summer, apart from a small period in late February when it is surpassed by 2020/21.

475 In 2017/18, 2018/19, 2019/20 and 2020/21 the polynya area has increased to between 25 439 km² (2017)
 476 and 38 310 km² (2020) by 1 December. From then the polynya continues to follow an overall increasing trend
 477 through December, with the polynya reaching its peak area in January in each of these years. In 2018/19 the peak
 478 area is substantially lower (61 113 km²) than in other years, and the polynya only maintains an area above 60 000
 479 km² for six days in late January and early February. 2018/19 records the lowest area in comparison to other years on
 480 every day between 4 December and 3 February. In 2017/18, 2019/20 and 2020/21 the polynya behaves in a similar
 481 manner through most the period, with no one of those years consistently recording a higher area, and each year
 482 reaching a peak-open area that approximately fills the whole ASP study area. However, polynya area in 2020/21

483 reaches its peak later (January), and its decline begins later (late February). Notably, in 2017/18 the polynya experi-
 484 ences a temporary rapid re-opening as it increases from just 5 977 km² on 15 March to 48 779 km² on 21 March.
 485 This is an 8.2 fold increase in 6 days, and it is followed by a rapid decline. The polynya had the highest daily mean
 486 area for summer (November-March) in 2016/17, at 62 616 km², and 2018/19 had the lowest, at 38 518 km². The
 487 mean daily area of 2017/18, 2019/20 and 2020/21 for summer was 44 013 km², 44 979 km² and 44 447 km², respec-
 488 tively.



489
 490 **Fig. 5.** Daily winter (April-October) polynya area for each winter 2017-2020 (solid), and the 4-year mean of the
 491 daily areas for the whole winter period, as measured from AMSR-2 SIC data (dashed).

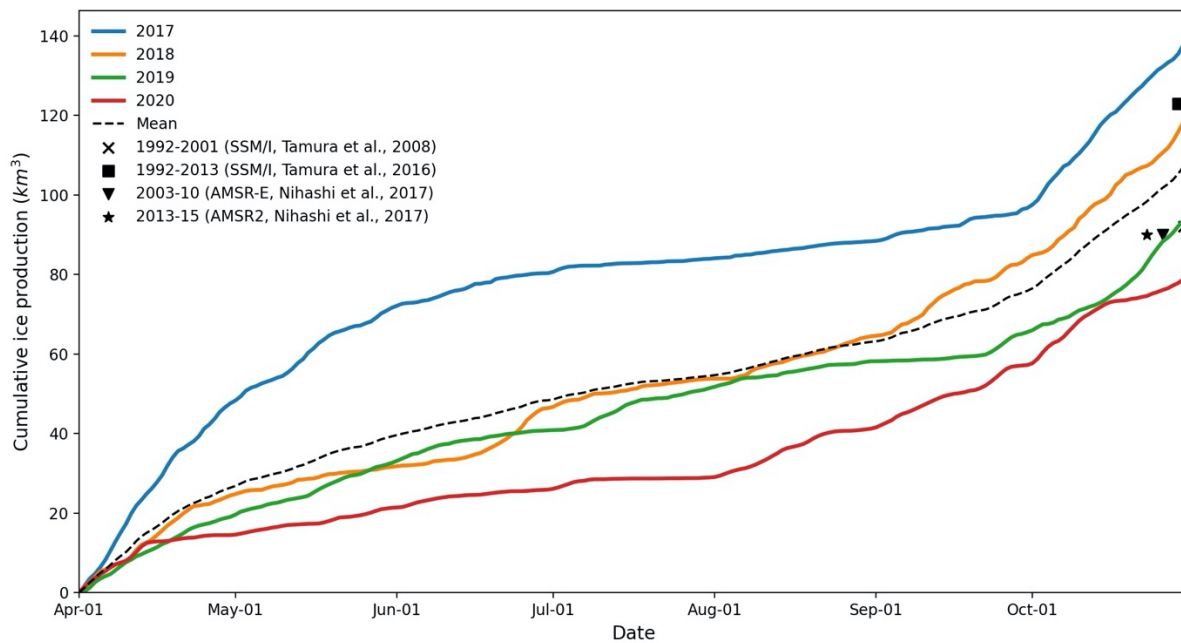
492
 493 **4.3 Winter Polynya Area and Ice Production**

494 In all years, polynya area exhibits an overall decline from the beginning of the winter period, when the po-
 495 lynya remains relatively large after the summer period (Fig. 5). This period, when the polynya remains relatively
 496 large but ice production has now begun, accounts for a substantial proportion of the annual ice production (Fig. 6;
 497 Fig. S4). On average, April/May accounts for 36% (39.6 km³) of annual ice production. The polynya then generally
 498 reaches a sustained winter low in area, where it fluctuates around and below 10 000 km². In 2020 the polynya area
 499 reaches its low in early April, while in 2017, 2019 and mean 2017-20 the area continues an overall decline through
 500 April, May and June. Polynya area and ice production then tend to remain low until an increase begins around Sep-
 501 tember. In July polynya area remains below 10 000 km² in all years for the whole month apart from brief small fluc-
 502 tuations above this in 2018 and 2019. There are notable spikes in polynya area in the middle of the year, which are
 503 also exhibited in spikes in ice production. Most notably in June in 2018 polynya area spikes to 26 631 km². After a
 504 period of low polynya area, the area generally increases through September and October towards the summer period.
 505 In 2020 this period of area and ice production increase begins in August. This late-winter increase in polynya area is

506 also exhibited in a corresponding marked increase in the rate of ice production. On average, September/October ac-
507 counts for 42% (45.8 km³) of annual ice production.

508 We note that in 2017 between the dates of 1 April and 8 May a substantial portion of the calculated active
509 polynya area, and ice production, occurs in the northwest of the ASP study area. This area is part of the open ocean
510 and is separated by sea ice from the more-typically active polynya area adjacent to the iceberg chain. Typically, ice-
511 pack fills this northwest area, but in early 2017 it is open due to the lack of icepack in this sector in the summer of
512 2016/17, discussed in section 4.3 (Video S2; Fig. 11b).

513 Analysis of the spatial distribution of ice production across all years reveals that the mean daily ice produc-
514 tion is highest in the area of the polynya adjacent to the Iceberg Chain, Thwaites Iceberg Tongue and Dotson Ice
515 Shelf (Fig. 7). Mean annual ice production values (April-October) in this region surpass 17 m³/m². Other notable
516 areas of higher ice production lie along various parts of the coast and an area that corresponds to the secondary po-
517 lynya by the Central Grounded Icebergs.



518
519
520 **Fig. 6.** Daily cumulative winter ice production for each winter (April-October) 2017-2020 (solid), and the 4-year
521 mean for the period (dashed), as measured using heat-flux modeling of ERA-5 data and AMSR-2 SIC data. Also
522 shown are mean annual measurements for 1992-2001 (Tamura et al., 2008), 1992-2013 (Tamura et al., 2016), 2003-
523 10 and 2013-15 (Nihashi et al., 2017), along with the instrument used for each measurement. Note the previous stud-
524 ies' measurements covered the period March-October and used a study area that does not exactly correspond to ours.
525

Year	Mean Daily Active Polynya Area (km ²)	Total Annual Ice Production (km ³)	Total Mean Daily Ice Production (km ³)
2017	10 908 (9589)	139	0.67 (0.67)
2018	9 963 (7004)	121	0.57 (0.50)
2019	8 152 (5127)	95	0.45 (0.38)
2020	6 910 (5692)	80	0.38 (0.36)
Mean 2017-20	8 984 (7240)	109	0.52 (0.51)

Table 2. Estimates of Mean Daily Active Polynya Area, Total Annual Ice Production and Mean Daily Ice Production during the winters of 2017-2020, and for the daily mean of the period. Numbers in brackets indicate the standard deviation.

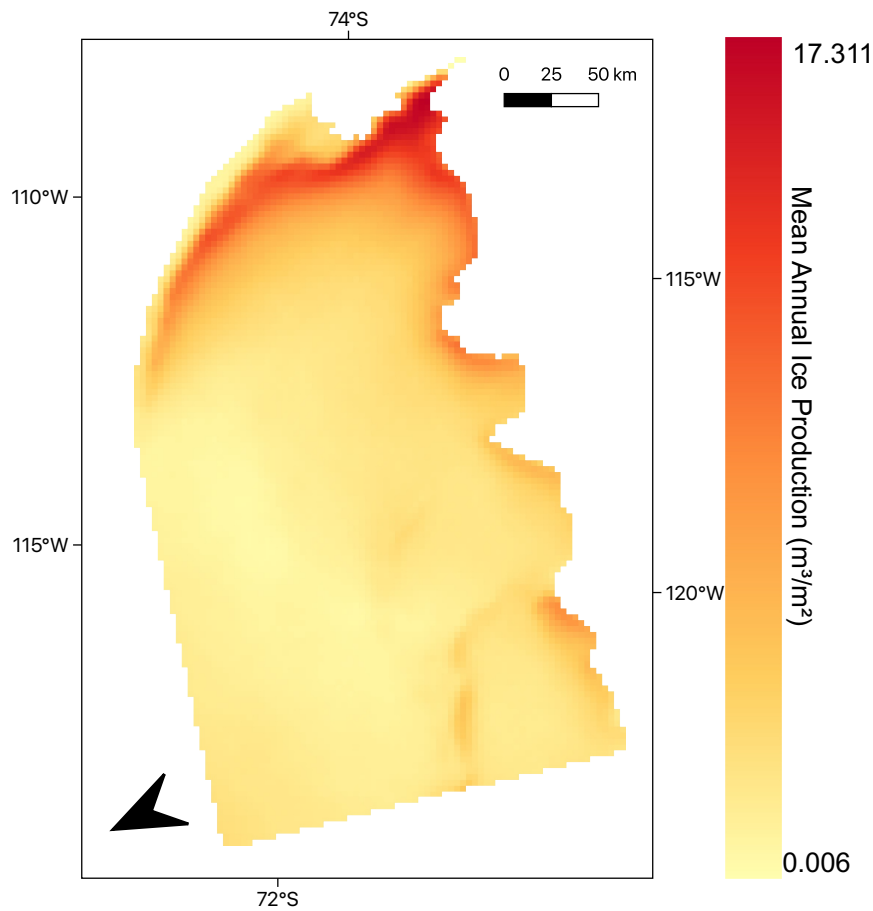


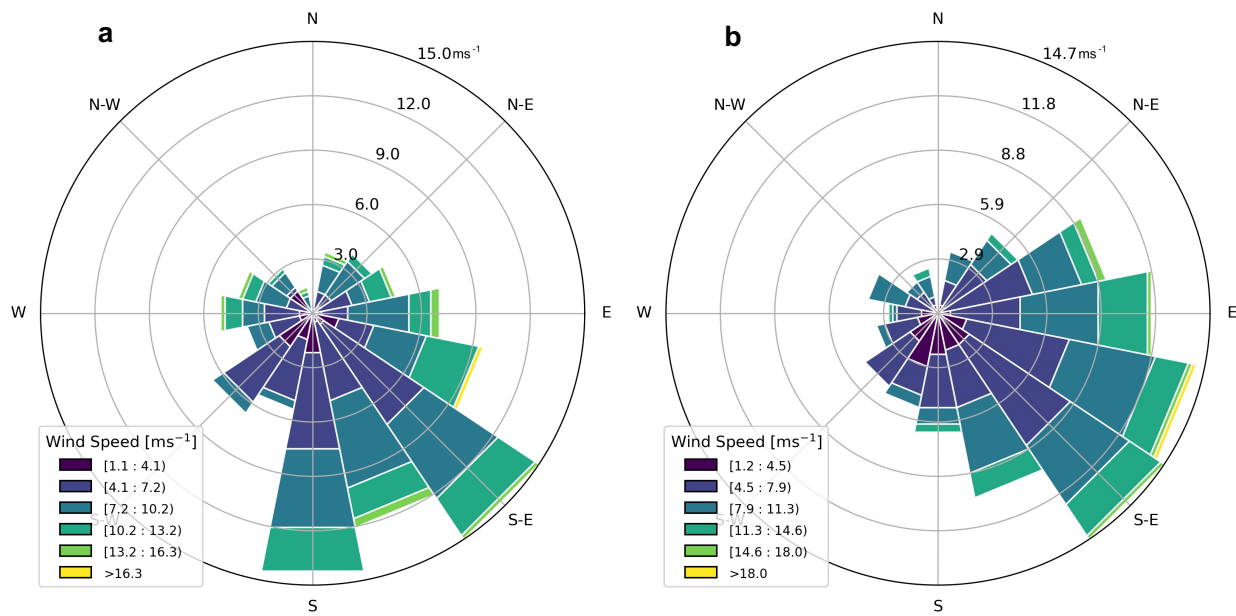
Fig. 7. Mean Annual Ice Production for all winter study periods (April-October 2017-2020). The region corresponds to the region within the green outline in Fig. 1b

526

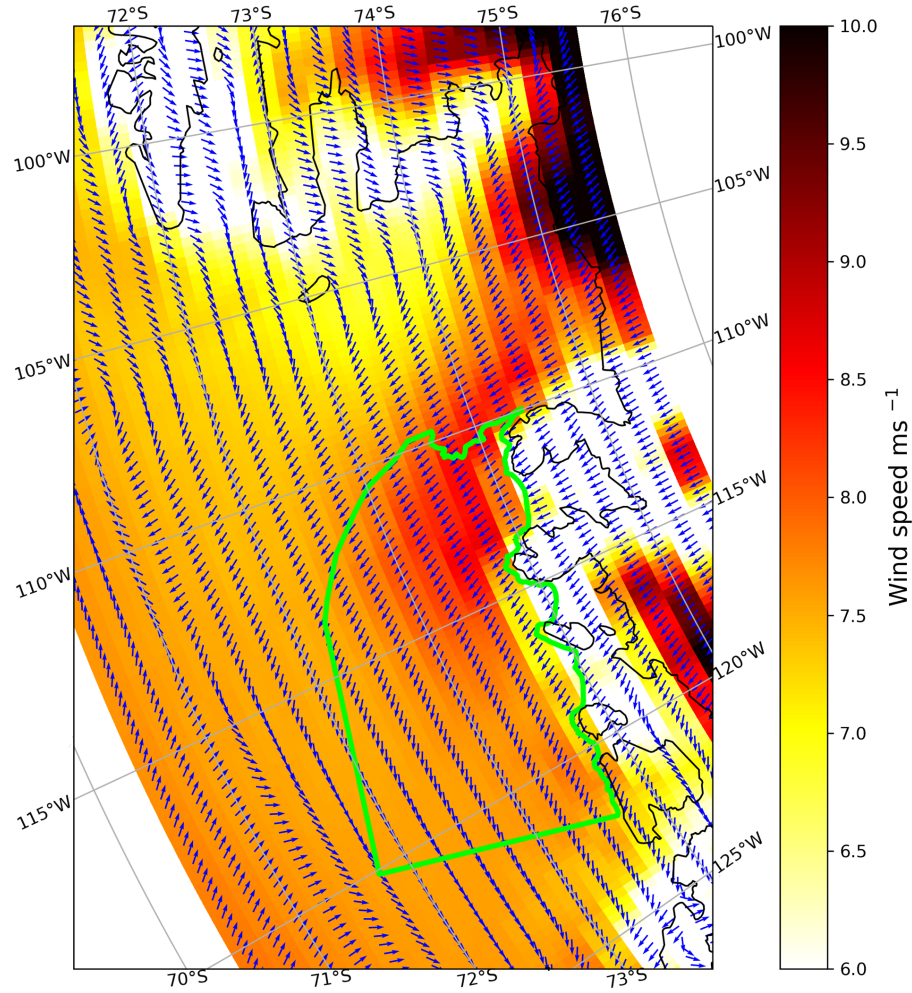
527

528 4.4 Wind and polynya area

529 Polynya events are associated with the presence of strong south-easterly and easterly winds in the region.
530 Figs. 8-9 show that south-easterly and easterly winds dominate the polynya study area. Comparing winter winds, in
531 the region where the polynya forms from (Fig. 8; S2), when the active polynya *does not* increase in area and when it
532 *does*, shows that while south-easterly winds often occur in both instances, there is a stronger easterly component
533 when an increase in area occurs. The top three wind directions associated with a daily increase in active polynya
534 area are south-easterly, east-south-easterly, and easterly, whereas they are south-easterly, southerly, and south-south-
535 easterly when area does not increase. Fig. S3 also shows the high density of active polynya area increases with
536 winds with a southerly/easterly winds. It is also visible in Fig. 9 that the location of polynya formation, adjacent to
537 the Dotson Ice Shelf, is associated with a band of high winds with a mean speed of around 8 – 9 ms⁻¹ that extends
538 along the coast from Thwaites Glacier, over the Thwaites Iceberg Tongue and into the south-eastern area of the ASP
539 study area. In the western part of the study area that the polynya extends into, winds tend to be more easterly than
540 south-easterly.
541



542
543 **Fig. 8.** Wind roses showing the distribution of wind speed and direction during all winters (April-October) in the
544 study period, when the active polynya (a) did not increase in area and (b) did increase in area. These winds are cal-
545 culated for a region close around that the iceberg chain that the polynya forms from, shown by Fig. S2.



546

547

548 **Fig. 9.** Annual mean vector wind field and wind speed, calculated for the period 1 November 2016 to 31 December

549 2020. The green boundary represents the ASP study area, also shown in Fig 1b. Daily maps of vector wind fields

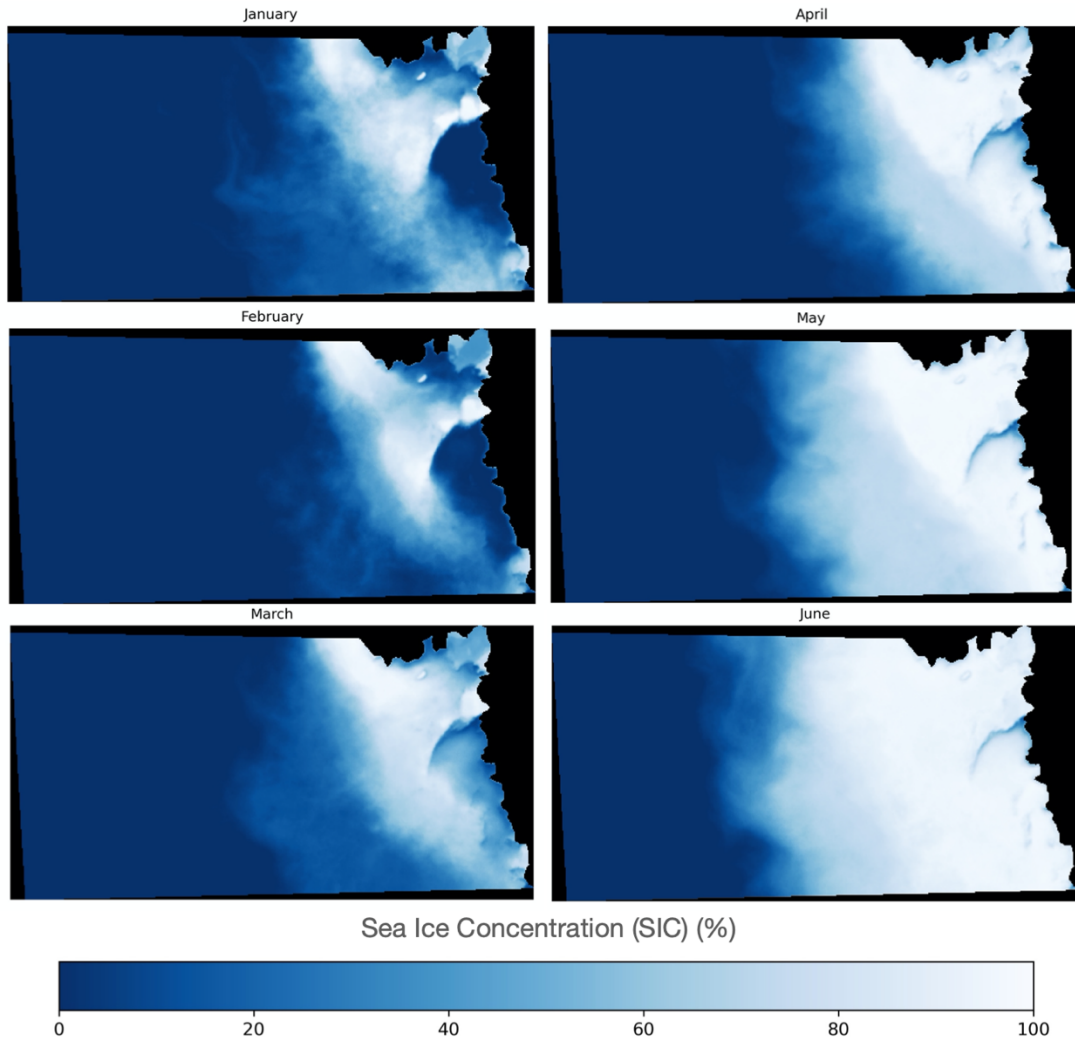
550 and wind speed are included as Video S3.

551

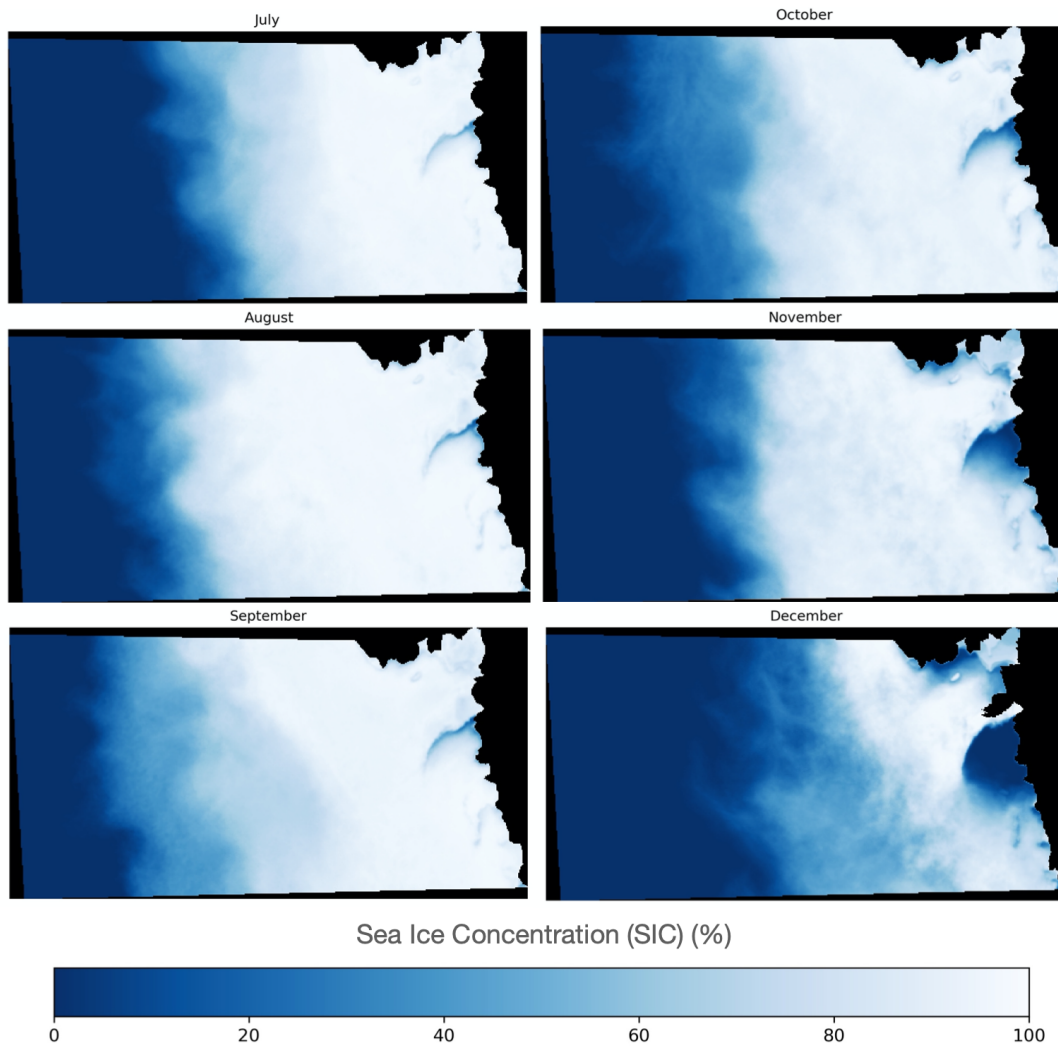
552

553

554

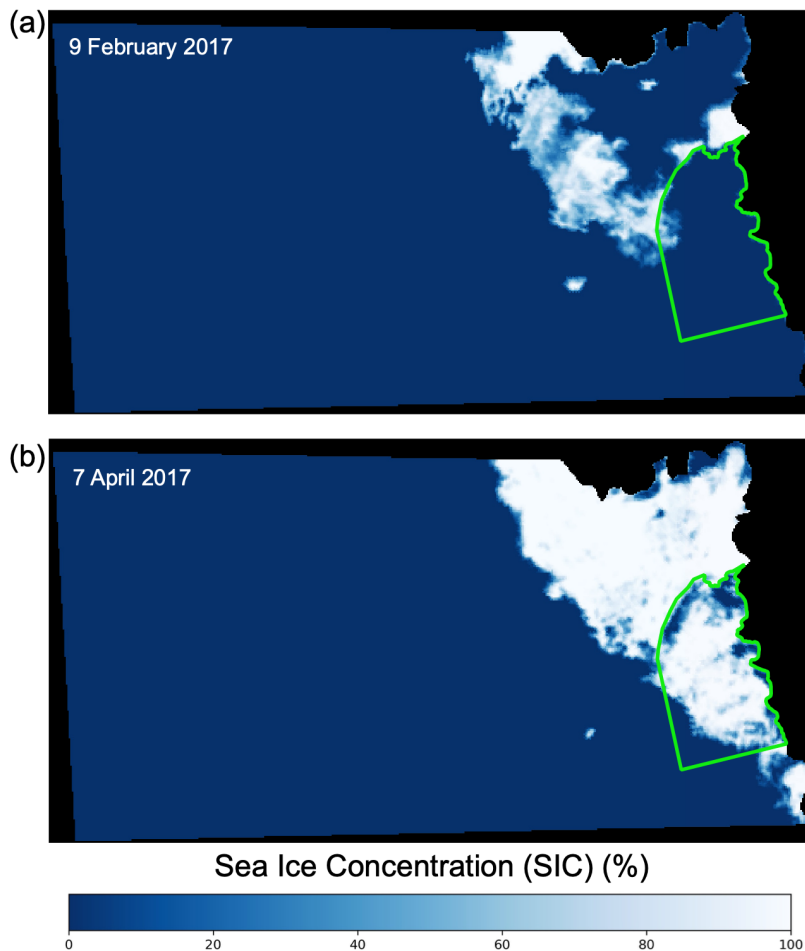


556
557
558
559
560
561
562
563
564
565
566
567
568
569



570 **Fig. 10.** Mean monthly SIC for the broader ASP region for the period November 2016 to March 2021. The area cor-
 571 responds to that shown by red box in Fig. 1a. Daily data is shown in Video S2.

572
 573
 574
 575
 576
 577
 578
 579
 580
 581
 582



584

585 **Fig. 11.** SIC for the broader ASP region on two days in 2017, during and following a summer of record-low SIC. (a)
 586 An example of when the polynya had no sea ice boundary to the west/north-west due to the exceptionally low SIC in
 587 the region during the 2016/17 summer. (b) An example of the low SIC in the region early in the subsequent winter,
 588 when only a narrow area of pack ice and polynya ice fills the area. The area corresponds to that shown by red box in
 589 Fig. 1a.

590

591 4.5 Broader SIC

592 Analysis of the SIC over a broader area also shows daily changes in the polynya area and how it relates to
 593 changes in the icepack. The mean monthly cycle of the polynya can be seen in Fig. 10 and presents a similar picture
 594 of the polynya as described in sections 4.1- 4.3. The broader icepack has a minimum total SIC in January and re-
 595 mains similar in February. From March the broader icepack can be seen to expand in area as the polynya begins to
 596 close and continues to increase until a peak SIC in September. From October the icepack begins a marked decline

597 into summer. Interannual variation can be seen in Fig. S5 and Video S2, with maximum icepack area occurring in
598 August or September each year, and minimum icepack in January or February.

599 During the summer of 2016/17 the icepack is notably sparse (Fig. 11; S5). Around 29 December 2016 a
600 gap in the icepack connects the ASP to the open ocean to north. The icepack continues to diminish and the gap con-
601 necting the ASP to the open ocean broadens until by February the polynya is only bound by part of the Iceberg
602 Chain and Thwaites Iceberg Tongue. The total SIC reaches a minimum on 5 February 2017, 35% of the next lowest
603 annual minimum (2019/20). Gaps in icepack around the Iceberg Chain mean that the ASP has essentially joined
604 with the Pine Island Polynya through the Iceberg Chain for a period in this year. The narrow band of icepack from
605 the east closes the polynya off again in March but the band of adjacent icepack remains so narrow that, as men-
606 tioned, there is open ocean inside our ASP study area until 9 May (Video S2).

607

608 **5. Discussion**

609 Our analysis shows that in some ways the ASP, between November 2016 and March 2021, behaves as is
610 typical for Antarctic coastal polynyas. During the summer the polynya becomes larger and remains ice-free (Fig. 4,
611 Video S1), while during the winter it becomes smaller, activating during ice-producing polynya ‘events’ (Figs. 4-5,
612 Video S1). These polynya events and changes in polynya area can sometimes be attributed to higher wind speeds
613 and are often associated with a stronger easterly component in winds close to the iceberg chain (Figs 7-9, S3).

614 Our qualitative analysis of Sentinel-1 SAR imagery, however, also reveals distinct characteristics of the
615 ASP which are not possible to decipher from sea ice concentration data, other quantitative methods, or indirect ob-
616 servation. First, we note that while in many other polynyas, such as the Ross Ice Shelf Polynya, new polynya-pro-
617 duced ice is typically efficiently evacuated away from its origin (Dai et al., 2020), this is not the case at the ASP.
618 Instead, ice formed by the ASP often remains in the ASP study area for months (Video S1). In fact, this polynya-
619 produced ice does not consistently flow in a direction away from the polynya. While its overall direction is west-
620 ward, away from the polynya, the ice ‘heaves’ and temporarily flows ‘backward’ (‘back-fills’) (Fig. 3), as has also
621 been observed at the Mertz Glacier Polynya (Massom et al., 2017). The ice also gets ‘stuck’ in the region, particu-
622 larly around grounded icebergs, which are grounded in areas where there are topographic highs in the sea floor (Fig.
623 2a, h).

624 The tendency of ice produced by the ASP to remain in the vicinity of the polynya for prolonged periods,
625 become stuck, and sometimes flow back eastward towards the site of its formation, influences the polynya and ice
626 production in two key ways. First, when ice moves back eastward while the polynya is active, it contributes to the
627 closure of the polynya, and thus the cessation of ice production. Typically, it is assumed that an active polynya dur-
628 ing winter closes due to new ice production (e.g. Cheng et al., 2017). However, the ASP may close both due to ice
629 production and movement of previously-produced ice into the polynya. Second, we suggest that the blockages of ice
630 in the vicinity of the polynya reduce the size and frequency of polynya events by hindering the ability of ice to move
631 out of the polynya and open it up. Again, by reducing the size and duration of active polynya area during winter, ice
632 production is limited.

633 We also note that the ASP forms along the coast westward off a chain of icebergs that extend from the
634 Thwaites Iceberg Tongue. While some polynyas, such as the Ross Ice Shelf polynya, form off and away from the
635 coast, the majority of Antarctic polynyas have been shown to form westward off glacier ice tongues or protruding
636 fast ice (Nihashi et al., 2017). In the case of the ASP, its location and orientation is determined by the presence of
637 the ‘Iceberg Chain’, which is in turn determined by the presence of a bathymetric high (Figs. 1-2). Stammerjohn et
638 al. (2015) refer to the polynya as forming off a ‘fast ice tongue’ but we prefer to refer to the ‘Iceberg Chain’ as the
639 eastern boundary. While a section of fast ice exists amongst, and adjacent to, a section of the southern part of the
640 Iceberg Chain, the extent of this fast ice varies and it only ever extends along a portion of the Iceberg Chain. The
641 Iceberg Chain remains virtually the same length throughout our observations. The polynya consistently forms off the
642 Iceberg Chain regardless of the state or extent of the fast ice. This means that, unlike polynyas that form off variable
643 fast ice (Nihashi et al., 2017), the fundamental morphology of the ASP remains stable through the period. We also
644 note that at no point do we observe significant portions of icepack to ‘break through’ the Iceberg Chain from the
645 east, regardless of the state of fast ice extent or conditions, and thus the icebergs and the bathymetric high persis-
646 tently ‘shield’ the polynya from icepack inflow.

647 Another notable feature of the ASP is the development of a ‘secondary polynya’ during the winter (Fig.
648 2a), where ice production also takes place. This is a polynya that forms within the ASP study area, in an area that is
649 usually part of the main ASP during the summer, but it is not typically congruent with the ‘main’ polynya during the
650 winter. The polynya forms at the site of the ‘Central Grounded Icebergs’ and associated ‘stuck’, transient fast ice.
651 Because some ice has become stuck over the bathymetric high, when adjacent ice drifts away a polynya activates.
652 This feature again highlights the significance of the bathymetry of the region for sea ice production and dynamics.

653 In line with previous studies of the ASP we find that the ASP is an important site of ice production
654 throughout the winter. Our estimates of annual ice production for 2018, 2019 and the mean for 2017-20 fall within
655 the estimations by Tamura et al. (2008; 2016) and Ohshima et al. (2017) for 1992-2001/2003-10/2013-15 (90 – 123
656 km³) (Fig. 6). Our estimates for total annual ice production for 2017 (139 km³) is higher than the highest estimate of
657 those studies, while for 2020 (80 km³) it is lower. This suggests no significant trend in interannual ice production
658 can be discerned from comparing the period of our study to these previous studies. Some caution must be used in
659 this comparison, however, because those studies include March in ice production calculations and our ASP study
660 area does not exactly correspond to theirs.

661 We find that the shoulder seasons of April/May and September/October are particularly important for ice
662 production due to the higher polynya area at these times, accounting for 36% and 42% of the annual ice production,
663 respectively. This is particularly the case in 2017, when an exceptionally high open polynya area in the summer, due
664 to low icepack conditions (discussed below), continues into the winter period (Figs. 4-6). However, we show that at
665 least some polynya area activates and some ice production occurs throughout the whole winter (Figs. 5-6). Addition-
666 ally, there can be spikes in polynya area and ice production in the deepest winter months. Most notably, polynya
667 area reaches 26 631 km² in June. Such isolated, winter events are not reflected in the daily mean for the whole study
668 period, but only when analyzing daily changes for each year (Fig. 5), highlighting the importance of analyzing po-
669 lynya area and ice production at the daily scale to discern important polynya dynamics.

670 When comparing our results to those of Cheng et al. (2017), who used the same method for calculating ice
671 production at the Ross Ice Shelf Polynya, we find that the ASP produces substantially less ice. Between 2003 and
672 2015 they found ice production for the Ross Ice Shelf Polynya was between 164 and 313 km³ (also for April - Octo-
673 ber) compared to 80 to 139 km³ for the Amundsen Sea Polynya (this study). This is in line with other studies that
674 compare the two polynyas (Tamura et al. 2008; 2016; Nihashi et al. 2017). We suggest that one limit on polynya
675 area and ice production for the ASP compared to the larger Ross Ice Shelf Polynya, is that the ASP typically forms
676 off the Iceberg Chain. The Iceberg Chain has a stable length of ~190 km, limited by the length of the seafloor sill on
677 which it is grounded, and is an upper limit on the polynya in one dimension. The Ross Ice Shelf Polynya, on the
678 other hand, forms off a coastline, and is only typically limited in this spatial dimension by weather/oceanographic
679 conditions. Another comparative limit on the ASP's ice production is the previously discussed tendency for po-
680 lynya-produced ice to inhibit further activation of the polynya due to blockages and reversals in ice drift. This pro-
681 cess could also partly explain why Cheng et al. (2017) found ice production to remain relatively consistent through-
682 out the winter for the Ross Ice Shelf Polynya, whereas we find ice production for the ASP in June-August to be
683 much lower than in the shoulder months of April/May and September/October.

684 We also note the polynya-produced ice exits our study area and enters the adjacent sector of the Amundsen
685 Sea to the west, rather than traveling away from the coast after formation. This westward flow of the ice away from
686 the polynya is likely, in this section, primarily due to the prevalence of easterly winds, especially towards the west-
687 ern part of the study area, and westward ocean currents in the region (Kim et al., 2016; St-Laurent et al., 2019).
688 These ocean currents have been shown to carry icebergs away from our study region, westward through the Amund-
689 sen Sea and into the Ross Sea (Koo et al., 2021). Broader prevailing easterly winds likely play a dominant role in
690 sea ice produced by the ASP eventually drifting to the Ross Sea, as part of a coastal band of westward ice drift (Ass-
691 mann et al., 2005). The fact that the polynya-produced ice remains by the coast may also be influenced by the inflow
692 of older, thicker icepack into our study area. Icepack appears to flow into the region from the Bellingshausen Sea
693 (Video S1, S2) and flows parallel to the ASP-produced ice, potentially playing some role in 'trapping' the ice by the
694 coast. The westward flow of the ice suggests that the level of ice production in the ASP is significant for the adja-
695 cent sector of the Amundsen Sea and the Ross Sea.

696 During the summer we observe the ASP to behave in a similar way in 2016/17 - 2020/21 as Stammerjohn
697 et al. (2015) showed for the period 1979 - 2014. As they did, we find the polynya to open every summer during our
698 study period. We do not note any shift in the location of opening, with the location remaining in the same place as
699 Stammerjohn et al. (2015) noted that it had shifted to in 1992/93. As they did for the years 1992, 1993, 1995, 1997,
700 2003, and 2010, we also note that in 2016/17, there is no icepack adjacent to the ASP in the north and west. This is
701 due to limited advection from the Bellingshausen Sea and Pine Island Polynya, and it causes the ASP to become
702 congruent with the open ocean (Fig. 11). This year was noted as a year of unprecedented springtime retreat and low
703 sea ice concentration for Antarctic sea ice, and was associated with a series of record atmospheric circulation anom-
704 alies and sea surface temperatures (Turner et al., 2017). These broader sea ice conditions caused the polynya to be
705 open in approximately the whole ASP study area through most of the summer in 2016/17, from late November to

706 March. During this time there is also little-to-no distinction between the ASP and the neighboring Pine Island Po-
707 lynya, other than the presence of the Iceberg Chain (Fig. 11a, Video S1). The effect of these extraordinary sea ice
708 conditions in 2016/17 on the polynya in summer, and early winter as mentioned above, may offer insight into how
709 the ASP will behave more commonly in the future if climate change makes such conditions more likely.

710 We note that while Stammerjohn et al. (2015) found the largest polynya area to be February in all but two
711 years during 1979 - 2014, we find the polynya area to be highest in January in each year apart from 2016/17 (when it
712 reaches the peak in November) (Fig. 4). Arrigo et al. (2012) also generally found the polynya area to increase until a
713 later peak in February for the years 1997/98 - 2009/10. While there should be some caution in directly comparing
714 our results with those, due to varying datasets, methods and definitions of the study area, we suggest that a shift in
715 the timing of maximum summer area would promote primary productivity in the polynya. Arrigo et al. (2012) found
716 primary productivity (per unit area) to typically peak in January, and to be declining by the time of the polynya area
717 peak. If the polynya reaches a higher area at an earlier time, when primary productivity is higher, we suggest the
718 potential for primary productivity may be larger during our study period.

719

720 **6. Conclusions**

721 Focusing on the summers of 2016/17 - 2020/21 and the winters of 2017 - 2020, we present the first detailed
722 study of year-round variations in the Amundsen Sea Polynya's behavior, area, and ice production. In particular, we
723 take advantage of the recent availability of Sentinel-1 SAR imagery to qualitatively assess the dynamics of the po-
724 lynya through the whole year.

725 Our findings agree with previous studies of earlier periods in finding that the ASP produces a substantial
726 amount of ice through the winter, with some inter-annual variation. We add that the shoulder seasons of April/May
727 and September/October dominate winter ice production, contributing a combined 78%. However, large polynya
728 events, often associated with high winds and a stronger easterly component in wind direction, can occur throughout
729 the winter, promoting significant ice production.

730 The ASP opens each summer in November and closes in March or early April, with peak area typically oc-
731 ccurring in January. We find that broader regional sea ice conditions can play an important role in the polynya in
732 summer, with the record-low sea ice extent in 2016/17 causing the ASP to become congruent with the open ocean to
733 the north and join with the Pine Island Polynya to the east.

734 Through our qualitative assessment we identify that the ASP behaves in a distinct manner. The polynya
735 typically forms in a westward direction off a persistent chain of grounded icebergs that are grounded along a bathy-
736 metric high. Ice produced by the polynya is not efficiently evacuated from the site as with other polynyas such as the
737 Ross Ice Shelf Polynya. Instead it stays within the study site, typically for months through the winter, sometimes
738 becoming stuck. This behavior is related to local topographic sea-floor highs which cause icebergs to become
739 grounded and ice to become stuck. At times another smaller 'secondary polynya' forms within the study area adja-
740 cent to grounded icebergs. Relatedly, ice produced by the polynya does not consistently move away from the ASP,
741 instead 'heaving' and sometimes drifting back towards it, contributing to its closure and limiting ice production. Un-
742 like some other polynyas, the polynya-produced ice also drifts westward into other sectors, instead of north, away

743 from the coast. These behaviors should be accounted for when considering the ASP's influence on the region's sea
744 ice, biology and oceanography.

745 Given temporal and spatial gaps in Sentinel-1 SAR's coverage, and the difficulty in automating polynya-
746 identification in SAR data, we do not find that it can replace passive microwave or sea ice concentration datasets for
747 analyzing daily changes in polynya area or ice production. However, we find that the ability to directly observe and
748 qualitatively analyze the polynya at a high spatial and temporal resolution, year-round, using Sentinel-1 imagery
749 provides important insights that are not possible with those other datasets. Development of automated approaches to
750 also use Sentinel-1 to quantify high-spatial resolution changes in polynya area and state, such as through machine-
751 learning, could extract more potential from the datasets, particularly for regions with fewer temporal and spatial
752 gaps. Combining such an approach with ice-tracking algorithms to track ice produced by polynya events and meas-
753 urements of ice thickness (e.g. from satellite altimetry), could help further quantify ice production by polynyas.

754

755 *Code and Data Availability*

756 Code for data processing and production of figures and videos is available at
757 <https://github.com/geogeordie/AmundsenSeaPolynyaPaper>. All processing was done with freely available software,
758 and all data is freely available. Sentinel-1 images were processed in Google Earth Engine or downloaded from:
759 asf.alaska.edu. BedMachine Antarctica V2 was downloaded from: <https://nsidc.org/data/nsidc-0756>. Sea ice concen-
760 tration data was downloaded from: <http://seaice.uni-bremen.de/>. ERA5 climate data was downloaded from:
761 <https://cds.climate.copernicus.eu>. The MODIS image used for Fig. 1b was downloaded from:
762 <https://worldview.earthdata.nasa.gov/>

763

764 *Video Supplement*

765 Video S1: <https://doi.org/10.5281/zenodo.5179444>

766 Video S2: <https://doi.org/10.5281/zenodo.5179509>

767 Video S3: <https://doi.org/10.5281/zenodo.5179590>

768

769 *Author Contributions*

770 GJM primarily conceived the study, processed and analyzed all data and produced all figures, apart from some of
771 the wind processing, analysis, and figures done by AB-C. SFA and AMM-N also contributed to the design of the
772 study and all authors discussed the results and were involved in editing the manuscript.

773

774 *Competing Interests*

775 The authors declare that they have no conflict of interest.

776

777 *Financial Support*

778 GJM, SFA and AMM-N were supported by NASA grant #80NSSC19M0194. AB-C was supported by NSERC
779 grant #RGPIN-2022-05217.

780

781 *Acknowledgements*

782 We gratefully acknowledge the European Space Agency for making available Sentinel-1 data and the SNAP
783 toolbox, and Google Earth Engine for hosting and processing Sentinel-1 data. We acknowledge the free package
784 Quantarctica, developed by the Norwegian Polar Institute, for use in Fig. 1a. We thank the University of Bremen
785 Sea Ice Remote Sensing Group for processing and making available their sea ice concentration product and the Japa-
786 nese Space Exploration Agency for launching and managing AMSR2. We also acknowledge the ECMWF, NSIDC
787 and NASA for freely-available data. Among others, the free, open-source software packages QGIS, GDAL, Python,
788 NumPy and Matplotlib were invaluable in this research. We also thank the GIS and StackOverflow StackExchange
789 communities for resources that aided data processing. We thank four anonymous reviewers who reviewed the paper
790 and editor Nicolas Jourdain for suggested revisions.

791

792 **References**

793 Armstrong, T.: World meteorological organization: WMO sea-ice nomenclature. Terminology, codes and illustrated
794 glossary. *J. Glaciol.*, 11, 148–149. <https://doi.org/10.3189/S0022143000022577>, 1972.

795
796 Arrigo, K. R., van Dijken, G. L., and Bushinsky, S.: Primary production in the Southern Ocean, 1997–2006, *J. Ge-*
797 *ophys. Res.*, 113, C08004. <https://doi.org/10.1029/2007JC004551>, 2008a.

798
799 Arrigo, K. R., van Dijken, G. L., and Long, M.: Coastal Southern Ocean: A strong anthropogenic CO₂ sink. *Ge-*
800 *ophys. Res. Lett.*, 35, L21602. <https://doi.org/10.1029/2008GL035624>, 2008b.

801
802 Arrigo, K. R., Lowry, K. E., and van Dijken, G. L.: Annual changes in sea ice and phytoplankton in polynyas of the
803 Amundsen Sea, Antarctica. *Deep Sea Research, II* 71–76: 5–15. <https://doi.org/10.1016/j.dsr2.2012.03.006>, 2012.

804
805 Arrigo, K. R. and van Dijken, G. L.: Phytoplankton dynamics within 37 Antarctic coastal polynya systems. *J. Ge-*
806 *ophys. Res.*, 108, 3271 <https://doi.org/10.1029/2002jc001739>, 2003.

807
808 Arthur, J. F., Stokes, C. R., Jamieson, S. S. R., Miles, B. W. J., Carr, J. R., and Leeson, A. A.: The triggers of the dis-
809 aggregation of Voyeykov Ice Shelf (2007), Wilkes Land, East Antarctica, and its subsequent evolution. *J. Glaciol.*
810 <https://doi.org/10.1017/jog.2021.45>, 2021.

811
812 Assmann, K. M., Hellmer, H. H., and Jacobs, S. S.: Amundsen Sea ice production and transport. *J. Geophys. Res.*,
813 110, C12013. <https://doi.org/10.1029/2004JC002797>, 2005.

814
815 Banwell, A. F., Willis, I. C., Macdonald, G. J., Goodsell, B., Mayer, D. P., Powell, A., and MacAyeal, D. R.: Calv-
816 ing and rifting on the McMurdo Ice Shelf, Antarctica. *Ann. Glaciol.*, 58, 78–87. <https://doi.org/10.1017/aog.2017.12>,
817 2017.

818
819 Bett, D. T., Holland, P. R., Naveira Garabato, A. C., Jenkins, A., Dutrieux, P., Kimura, S., and Fleming, A.: The im-
820 pact of the Amundsen Sea freshwater balance on ocean melting of the West Antarctic Ice Sheet. *J. Geophys. Res.:*
821 *Oceans*, 125, e2020JC016305. <https://doi.org/10.1029/2020JC016305>, 2020.

822
823 Bracegirdle, T. J.: Climatology and recent increase of westerly winds over the Amundsen Sea derived from six rea-
824 nalyzes. *Int. J. Climatol.*, 33, 843–851. <https://doi.org/10.1002/joc.3473>, 2013.

825
826 Bromwich, D. H. and Kurtz, D. D.: Katabatic wind forcing of the Terra Nova Bay polynya. *J. Geophys. Res.*, 89,
827 3561. <https://doi.org/10.1029/JC089iC03p03561>, 1984.

828

829 Bromwich, D., Liu, Z., Rogers, A. N., and Van Woert, M. L.: Winter atmospheric forcing of the Ross Sea polynya.
830 Ocean ICE Atmos. Int. Antarct. Cont. Margin, 75, 101-133. <https://doi.org/10.1029/AR075p0101>, 1998.
831

832 Bromwich, D. H., Carrasco, J. F., Liu, Z., and Tzeng, R. Y.: Hemispheric atmospheric variations and oceanographic
833 impacts associated with katabatic surges across the ross ice shelf, Antarctica. J. Geophys. Res.-Atmos, 98, 13045-
834 13062. <https://doi.org/10.1029/93JD00562>, 1993.
835

836 Budge, J. S. and Long, D. G.: A comprehensive database for Antarctic iceberg tracking using scatterometer data.
837 IEEE JSTARS 11(2), 434-442. <https://10.0.4.85/JSTARS.2017.2784186>, 2018.
838

839 Cheng, Z., Pang, X., Zhao, X., and Tan, C.: Spatio-Temporal Variability and Model Parameter Sensitivity Analysis
840 of Ice Production in Ross Ice Shelf Polynya from 2003 to 2015. Remote Sensing, 9, 934.
841 <https://doi.org/10.3390/rs9090934>, 2017.
842

843 Cheng, Z., Pang, X., Zhao, X., and Stein, A.: Heat Flux Sources Analysis to the Ross Ice Shelf Polynya Ice Produc-
844 tion Time Series and the Impact of Wind Forcing, Remote Sensing, 11, 188. <https://doi.org/10.3390/rs11020188>,
845 2019.
846

847 Dai, L., Xie, H., Ackley, S. F., and Mestas-Nuñez, A. M.: Ice Production in Ross Ice Shelf Polynyas during 2017–
848 2018 from Sentinel–1 SAR Images. Remote Sensing, 12, 1484. <https://doi.org/10.3390/rs12091484>, 2020.
849

850 Doherty, B. T. and Kester, D. R.: Freezing Point of Seawater. J. Mar. Res., 32, 285-300. 1974.
851

852 Drucker, R., Martin, S., and Kwok, R.: Sea ice production and export from coastal polynyas in the Weddell and
853 Ross Seas. Geophys. Res. Lett., 38, L1705. <https://doi.org/10.1029/2011GL048668>, 2011.
854

855 Environment Canada.: Manual of Standard Procedures for Observing and Reporting Ice Conditions (MANICE), Me-
856 teorological Service of Canada, 2005. [Available at: https://publications.gc.ca/collections/collection_2013/ec/En56-175-2005-eng.pdf]
857
858

859 Greene, C. E., Young, D. A., Gwyther, D. E., Galton-Fenzi, B. E., and Blankenship, D. D.: Seasonal dynamics of
860 Totten Ice Shelf controlled by sea ice buttressing. Cryosphere, 12, 2869-2882. <https://doi.org/10.5194/tc-12-2869-2018>, 2018.
861
862

863 Grossmann, S. and Dieckmann, G. S.: Bacterial Standing Stock, Activity, and Carbon Production during Formation
864 and Growth of Sea–Ice in the Weddell Sea, Antarctica. Appl. Environ. Microb., 60, 2746–2753.
865 <https://doi.org/10.1128/aem.60.8.2746-2753.1994>, 1994.
866

867 Hersbach, H., Bell, B., Berrisford, P., Biavati, G., Horányi, A., Muñoz Sabater, J., Nicolas, J., Peubey, C., Radu, R.,
868 Rozum, I., Schepers, D., Simmons, A., Soci, C., Dee, D., and Thépaut, J.-N.: ERA5 monthly averaged data on single
869 levels from 1979 to present. Copernicus Climate Change Service (C3S) Climate Data Store (CDS). (Accessed on <
870 01-04-2021), <https://doi.org/10.24381/cds.fl7050d7>, 2019.
871

872 Hollands, T. and Dierking, W.: Dynamics of the Terra Nova Bay Polynya: The potential of multi-sensor satellite
873 observations, Remote Sens. Environ., 187, 30–48, <https://doi.org/10.1016/j.rse.2016.10.003>, 2016
874

875 IMBIE team: Mass balance of the Antarctic ice sheet from 1992 to 2017. Nature 558, 219-222.
876 <https://doi.org/10.1038/s41586-018-0179-y>, 2018.
877

878 Ito, M., Ohshima, K. I., Fukamachi, Y., Mizuta, G., Kusumoto, Y., and Nishioka, J.: Observations of frazil ice for-
879 mation and upward sediment transport in the Sea of Okhotsk: A possible mechanism of iron supply to sea ice. J. Ge-
880 ophys. Res.–Oceans, 122, 788–802. <https://doi.org/10.1002/2016JC012198>, 2017.
881

882 Kim, C.-S., Kim, K.-W., Cho, K.-H., Ha, H. K., Lee, S.H., Kim, H.-C., Lee, J.-H.: Variability of the Antarctic
883 Coastal Current in the Amundsen Sea. Estuar. Coast. Shelf S., 181, 123–133,
884 <https://doi.org/10.1016/j.ecss.2016.08.004>, 2016.

885
886 Kimura, N. and Wakatsuchi, M.: Increase and decrease of sea ice area in the Sea of Okhotsk: Ice production in
887 coastal polynyas and dynamic thickening in convergence zones. *J. Geophys. Res.-Oceans*, 109, C09S03.
888 <https://doi.org/10.1029/2003JC001901>, 2004.
889
890 Koo, Y., Xie, H., Ackley, S. F., Mestas-Nuñez, A. M., Macdonald, G. J., and Hyun, C.-U.: Semi-automated tracking
891 of iceberg B43 using Sentinel-1 SAR images via Google Earth Engine. *Cryosphere.*, 15, 4727–4744,
892 <https://doi.org/10.5194/tc-15-4727-2021>, 2021.
893
894 Lee, S.H., Hwang, J., Ducklow, H. W., Hahm, D., Lee, S. H., Kim, D., Hyun, J.-H., Park, J., Ha, H. K., Kim, T. W.,
895 Yang, E. J., Shin, H. C.: Evidence of minimal carbon sequestration in the productive Amundsen Sea polynya, *Ge-*
896 *ophys. Res. Lett.*, 44, 15, 7892-7899. <https://doi.org/10.1002/2017GL074646>, 2017.
897
898 Massom, R. A., Hill, K. L., Lytle, V. I., Worby, A.P., Paget, M. J., and Allison, I.: Effects of regional fast-ice and
899 iceberg distributions on the behaviour of the Mertz Glacier polynya, East Antarctica. *Ann. Glaciol.*, 33, 391-398.
900 <https://doi.org/10.3189/172756401781818518>, 2001.
901
902 Massom, R. A., Scambos, T. A., Bennetts, L. G., Reid, P., Squire, V. A., and Stammerjohn, S. E.: Antarctic ice shelf
903 disintegration triggered by sea ice loss and ocean swell. *Nature*, 558, 383-389. [https://doi.org/10.1038/s41586-018-](https://doi.org/10.1038/s41586-018-0212-1)
904 [0212-1](https://doi.org/10.1038/s41586-018-0212-1), 2018.
905
906 Matsuoka, K., Skoglund, A., Roth, G., de Pomereu, J., Griffiths, H., Headland, R., Herried, B., Katsumata, K., Le
907 Brocq, A., Licht, K., Morgan, F., Neff, P. D., Ritz, C., Scheinert, M., Tamura, T., Van de Putte, A., van den Broeke,
908 M., von Deschanden, A., Deschamps-Berger, C., Van Liefferinge, B., Tronstad, S., and Melvær, Y.: Quantarctica,
909 an integrated mapping environment for Antarctica, the Southern Ocean, and sub-Antarctic islands. *Environ. Modell.*
910 *Softw.*, 140, 105015. <https://doi.org/10.1016/j.envsoft.2021.105015>, 2021.
911
912 Mazur, A. K., Wählín, A. K., Krężel, A.: An object-based SAR image iceberg detection algorithm applied to the
913 Amundsen Sea, *Remote Sens. Environ.*, 189, 67–83, <https://doi.org/10.1016/j.rse.2016.11.013>, 2017.
914
915 Mazur, A. K., Wählín, A. K., and Kalén, O.: The life cycle of small-to medium-sized icebergs in the Amundsen sea
916 embayment, *Polar Res.*, 38, 1–17, <https://doi.org/10.33265/polar.v38.3313>, 2019.
917
918 Moore, G. W. K., Howell, S. E. L., and Brady, M.: First observations of a transient polynya in the Last Ice Area
919 north of Ellesmere Island. *Geophys. Res. Lett.*, 48, e2021GL095099. <https://doi.org/10.1029/2021GL095099>, 2021.
920
921 Morales Maqueda, M. A., Willmott, A. J., and Biggs, N. R. T.: Polynya dynamics: a review of observations and
922 modeling, *Rev. Geophys.*, 42, RG1004. <https://doi.org/10.1029/2002RG000116>, 2004.
923
924 Morelli, S. and Parmiggiani, F.: Wind over Terra Nova Bay (Antarctica) during a polynya event: Eta model simula-
925 tions and satellite microwave observations. *Eur. Phys. J. Plus* 128, 135 (2013). [https://doi.org/10.1140/epjp/i2013-](https://doi.org/10.1140/epjp/i2013-13135-8)
926 [13135-8](https://doi.org/10.1140/epjp/i2013-13135-8), 2013.
927
928 Morlighem, M.: MEaSUREs BedMachine Antarctica, Version 2. Boulder, Colorado USA. NASA National Snow
929 and Ice Data Center Distributed Active Archive Center. <https://doi.org/10.5067/C2GFER6PTOS4>, 2019. [Date Ac-
930 cessed: 01-04-2021].
931
932 Nakata, K., Ohshima, K. I., and Nihashi, S.: Estimation of thin ice thickness and discrimination of ice type from
933 AMSR-E passive microwave data. *IEEE TGRS*, 57(1), 263–276. <https://doi.org/10.1109/TGRS.2018.2853590>,
934 2019.
935
936 Nakata, K., Ohshima, K. I., and Nihashi, S.: Mapping of active frazil for Antarctic coastal polynyas, with an estima-
937 tion of sea-ice production. *Geophys. Res. Lett.*, 48, e2020GL091353. <https://doi.org/10.1029/2020GL091353>, 2021.
938

939 Nihashi, S., and Ohshima, K. I.: Circumpolar Mapping of Antarctic Coastal Polynyas and Landfast Sea Ice: Relationship and Variability, *J. Climate*, 28, 3650-3670. <https://doi.org/10.1175/JCLI-D-14-00369.1>, 2015.

940

941

942 Nihashi, S., Ohshima, K. I., and Tamura, T.: Sea-Ice Production in Antarctic Coastal Polynyas Estimated From

943 AMSR2 Data and Its Validation Using AMSR-E and SSM/I-SSMIS Data. *IEEE JSTARS*, 10, 3912-3922.

944 <https://doi.org/10.1109/JSTARS.2017.2731995>, 2017.

945

946 Ohshima, K. I., Fukamachi, Y., Williams, G. D., Nihashi, S., Roquet, F., Kitade, Y., Tamura, T., Hirano, D., Her-

947 raiz-Borreguero, L., Field, I., Hindell, M., Aoki, S. and Wakatsuchi, M. L.: Antarctic Bottom Water production by

948 intense sea-ice formation in the Cape Darnley polynya. *Nat. Geosci.*, 6, 235-240. <https://doi.org/10.1038/ngeo1738>,

949 2013.

950

951 Park, J., Kim, H.-C., Jo, Y.-H., Kidwell, A., and Hwang, J.: Multi-temporal variation of the ross sea polynya in re-

952 sponse to climate forcings. *Polar Res.*, 37, 1444891. <https://doi.org/10.1080/17518369.2018.1444891>, 2018.

953

954 Parkinson, C. L.: A 40-y record reveals gradual Antarctic sea ice increases followed by decreases at rates far exceed-

955 ing the rates seen in the Arctic. *P. Natl. Acad. Sci. U.S.A.*, 116, 14414-14423.

956 <https://doi.org/10.1073/pnas.1906556116>, 2019.

957

958 Parmiggiani, F.: Fluctuations of Terra Nova Bay polynya as observed by active (ASAR) and passive (AMSR-E) mi-

959 crowave radiometers, *Int. J. Remote. Sens.*, 27:12, 2459 2467. <https://doi.org/10.1080/01431160600554355>, 2007.

960

961 Preußner, A., Heinemann, G., Willmes, S., and Paul, S.: Multi-Decadal Variability of Polynya Characteristics and Ice

962 Production in the North Water Polynya by Means of Passive Microwave and Thermal Infrared Satellite Imagery.

963 *Remote Sensing*, 7, 15844-15867. <https://doi.org/10.3390/rs71215807>, 2015.

964

965 [QGIS.org](http://www.qgis.org): QGIS Geographic Information System. QGIS Association. <http://www.qgis.org>. 2021.

966

967 Rack, W., Price, D., Haas, C., Langhorne, P. J., and Leonard, G. H.: Sea Ice Thickness in the Western Ross Sea. *Ge-*

968 *ophys. Res. Lett.*, 48, e2020GL090866. <https://doi.org/10.1029/2020GL090866>, 2020.

969

970 Rignot, E., Mouginot, J., Scheuchl, B., van den Broeke, M., van Wessel, M. J., and Morlighem, M.: Four decades

971 of Antarctic ice sheet mass balance from 1979–2017. *P. Natl. Acad. Sci. U.S.A.* 116, 1095-1103.

972 <https://doi.org/10.1073/pnas.1812883116>, 2019.

973

974 Sansiviero, M., Morales Maqueda, M. Á., Fusco, G., Aulicino, G., Flocco, D., and Budillon, G.: Modelling sea ice

975 formation in the Terra Nova Bay polynya. *J. Marine Syst.*, 166, 4-25. <https://doi.org/10.1016/j.jmarsys.2016.06.013>,

976 2017.

977

978 Spreen, G. Kaleschke, G. L., and Heygster, G.: Sea ice remote sensing using AMSR-E 89 GHz channels. *J. Geophys.*

979 *Res.*, 113, C02S03. <https://doi.org/10.1029/2005JC003384>, 2008.

980

981 Stammerjohn, S. E., Maksym, T., Massom, R. A., Lowry, K. E., Arrigo, K. R., Yuan, X., Raphael, M., Randall-

982 Goodwin, E. R., Sherrell, R. M., and Yager, P. L.: Seasonal sea ice changes in the Amundsen Sea, Antarctica, over

983 the period of 1979–2014. *Elementa: Science of the Anthropocene*, 3, 000055. <https://doi.org/10.12952/journal.ele->

984 [menta.000055](https://doi.org/10.12952/journal.elementa.000055), 2015.

985

986 St-Laurent, P., Yager, P. L., Sherrell, R. M., Stammerjohn, S. E., and Dinniman, M. S.: Pathways and supply of dis-

987 solved iron in the Amundsen Sea (Antarctica), *J. Geophys. Res.-Oceans*, 122, 7135–7162, [https://doi.org/10.1002/](https://doi.org/10.1002/2017JC013162)

988 [2017JC013162](https://doi.org/10.1002/2017JC013162), 2017.

989

990 St-Laurent, P., Yager, P. L., Sherrell, R. M., Oliver, H., Dinniman, M. S., and Stammerjohn, S. E.: Modeling the

991 seasonal cycle of iron and carbon fluxes in the Amundsen Sea Polynya, Antarctica. *J. Geophys. Res.: Oceans*, 124,

992 1544–1565. <https://doi.org/10.1029/2018JC014773>, 2019.

993

994 Sweeney, C.: The annual cycle of surface water CO₂ and O₂ in the Ross Sea: A model for gas exchange on the con-
995 tinental shelves of Antarctica, in *Biogeochemistry of the Ross Sea*. Antarctica Research Series, 78, edited by Dun-
996 bar, R. B., and DiTullio, G. R., pp. 295-312, AGU, Washington, D. C., 2003.
997
998 Tamura, T., Ohshima, K. I., and Nihashi, S.: Mapping of sea ice production for Antarctic coastal polynyas, *Ge-*
999 *ophys. Res. Lett.*, 35, L07606. <https://doi.org/10.1029/2007GL03290>, 2008.
1000
1001 Tamura, T., Williams, G. D., Fraser, A. D., and Ohshima, K. I.: Potential regime shift in decreased sea ice produc-
1002 tion after the Mertz Glacier calving. *Nat. Commun.*, 3, 826. <https://doi.org/10.1038/ncomms1820>, 2012.
1003
1004 Tian, L., Xie, H., Ackley, S. F., Tang, J., Mestas-Nuñez, A. M., and Wang, X.: Sea-ice freeboard and thickness in
1005 the Ross Sea from airborne (IceBridge 2013) and satellite (ICESat 2003-2008) observations. *Ann. Glaciol.*, 61(82),
1006 24-39. <https://doi.org/10.1017/aog.2019.49>, 2020.
1007
1008 Webber, B. G. M., Heywood, K. J., Stevens, D. P., Dutrieux, P., Povl Abrahamsen, E., Jenkins, A., Jacobs, S. S.,
1009 Ha, H. K., Lee, S. H., and Kim, T. W.: Mechanisms driving variability in the ocean forcing of Pine Island Glacier,
1010 *Nat. Commun.*, 8, 14507. <https://doi.org/10.1038/ncomms14507>, 2017.